Differential spatiotemporal targeting of *Toxoplasma* and *Salmonella* by GBP1 assembles caspase signalling platforms

Daniel Fisch[1,5], Barbara Clough[1], Marie-Charlotte Domart[2], Hironori Bando[3,4], Tereza Masonou[5], Lucy M Collinson[2], Masahiro Yamamoto[3,4], Avinash R Shenoy[5,6], Eva-Maria Frickel[1]

[1] Host-*Toxoplasma* Interaction Laboratory, The Francis Crick Institute, London, UK
[2] Electron Microscopy Science Technology Platform, The Francis Crick Institute, London, UK
[3] Department of Immunoparasitology, Research Institute for Microbial Diseases, Osaka University, Osaka, Japan
[4] Laboratory of Immunoparasitology, WPI Immunology Frontier Research Center, Osaka University, Osaka, Japan
[5] MRC Centre for Molecular Bacteriology & Infection, Department of Infectious Disease, Imperial College London, London, UK
[6] The Francis Crick Institute, London, UK

Human guanylate binding proteins (GBPs), a family of IFNγ-inducible GTPases, promote cell-intrinsic defence against pathogens and host cell death. We previously identified GBP1 as a mediator of cell death of human macrophages infected with *Toxoplasma gondii* (*Tg*) or *Salmonella Typhimurium* (STm). How GBP1 targets microbes for AIM2 activation during *Tg* infection and caspase-4 during STm infection remains unclear. Here, using correlative light and electron microscopy and EdU labelling of *Tg*-DNA, we reveal that GBP1-decorated parasitophorous vacuoles (PVs) lose membrane integrity and release *Tg*-DNA for detection by AIM2-ASC-CASP8. In contrast, differential staining of cytosolic and vacuolar STm revealed that GBP1 does not contribute to STm escape into the cytosol but decorates almost all cytosolic STm leading to the recruitment of caspase-4. Caspase-5, which can bind LPS and whose expression is upregulated by IFNγ, does not target STm pointing to a key role for caspase-4 in pyroptosis. We also uncover a regulatory mechanism involving the inactivation of GBP1 by its cleavage at Asp192 by caspase-1. Cells expressing non-cleavable GBP1^{D192E} therefore undergo higher caspase-4-driven pyroptosis during STm infection. Taken together, our comparative studies elucidate microbe-specific spatiotemporal roles of GBP1 in inducing cell death by leading to assembly and regulation of divergent caspase signalling platforms.

Caspase-1 | Caspase-4 | Caspase-8 | Pyroptosis | Apoptosis | Inflammasome | GBP1

Correspondence: eva.frickel@crick.ac.uk, a.shenoy@imperial.ac.uk

INTRODUCTION

Most nucleated cells have the ability to defend themselves against infection by viruses, bacteria and eukaryotic parasites in a process called cell-intrinsic immunity. The execution of this process requires the detection of pathogens by membrane-bound and cytosolic sensors and receptors, several of which can also trigger cell death (MacMicking, 2012; Randow *et al*, 2013; Mostowy & Shenoy, 2015; Jorgensen *et al*, 2017).The type II interferon, IFNγ, induces expression of up to 2000 interferon-stimulated genes by signalling via the interferon-gamma receptor signalling cascade (MacMicking, 2012). Several newly expressed proteins are involved in killing of or restricting the replication of intracellular pathogens or in inducing host cell death. The guanylate binding protein (GBP) family of cytosolic GTPases are among the most highly expressed proteins in macrophages exposed to IFNγ. The GBP protein family consists of seven members in the human and is involved in defence against bacterial, parasitic and viral intracellular pathogens, regulation of inflammasome signalling and cell death (Shenoy *et al*, 2012; Man *et al*, 2017; Santos & Broz, 2018; Gomes *et al*, 2019). All seven human GBPs possess an N-terminal, globular GTPase domain and a C-terminal helical domain which facilitates membrane interaction. Furthermore, GBP1, GBP2 and GBP5 are isoprenylated at their C-terminal CaaX-box, which can anchor them to membranes. GTPase activity mediates GBP conformational changes and hetero- and homo-oligomerization (Praefcke, 2018). However, recent studies have pointed towards pathogen-specific effects of GBPs and their roles in differentially triggering cell death needs to be better understood (Fisch *et al*, 2019a).

Starting with a family-wide siRNA screen, we showed that GBP1 is essential in macrophage cell death in response to infection by *Toxoplasma gondii* (*Tg*), an apicomplexan parasite, and *Salmonella enterica subsp. enterica* serovar Typhimurium (STm), a Gram-negative bacterium. GBP1 targeting of both pathogens is necessary for cell death. GBP1 localisation to these divergent pathogens leads to the exposure of pathogen-associated molecular patterns (PAMP), namely *Tg*-DNA and STm-LPS, which are detected by their cytosolic receptors AIM2 and caspase-4 respectively. As *Tg* induces the loss of inflammasome proteins, including NLRP3 and caspase-1, human macrophages undergo atypical apoptosis through the assembly of AIM2-ASC-caspase-8 complexes. On the other hand, GBP1 promotes caspase-4 activation and enhances pyroptosis during STm infection (Fisch *et al*, 2019a).

Human macrophages can detect pathogen DNA through either AIM2 or through a newly described NLRP3-mediated pathway in response to pathogens such as *Francisella novicida* and Modified vaccinia Ankara (Gaidt *et al*, 2016). Whether human AIM2 is specifically activated through the detection of *Tg*-DNA remains to be experimentally demonstrated. Similarly, whether caspase-4 is activated by vacuolar or cytosolic STm targeting by GBP1 is not known. As GBP1 targeting of different pathogens elicits divergent host cell death programs, we sought to investigate the mechanistic details of GBP1 during infection by these two unrelated human pathogens. Additionally, GBP1 contains a previously reported caspse-1 cleavage site (Naschberger *et al*, 2017), thus leading us to hypothesise that GBP1 not only differentially recognises dissimilar microbes to liberate PAMPs, but also provides a functional platform to feedback on the level of caspase activation.

In the current study, we used correlative light and electron microscopy and super-resolution microscopy to delineate the vacuolar compartments targeted by GBP1 and describe how GBP1 promotes the assembly of supramolecular organizing centres (SMOCs) as signalling platforms. Furthermore, we show how cleavage of GBP1 by caspase-1 functions as a negative feedback to balance cell death levels. Overall, we show that GBP1 has unique roles during infection by *Tg* or STm and thereby provide new insights on its role in host defence.

RESULTS

GBP1 directly contributes to *Toxoplasma* vacuole opening and infection control

GBP1 is recruited to *Tg* parasitophorous vacuoles (PV) which results in AIM2 and caspase-8 activation (Fisch *et al*, 2019a). Like some murine (Yamamoto *et al*, 2012; Selleck *et al*, 2013; Degrandi *et al*, 2013; Kravets *et al*, 2016), we hypothesized that human GBP1 may promote vacuole opening and cytosolic access to intravacuolar pathogens. To test this, we designed a new assay to quantify *Tg* vacuole opening. The cytosolic dye CellMask is excluded from PVs but enters the PV once the PV membrane (PVM) is disrupted by detergent-mediated permeabilization (**Figure S1A**). Increased dye intensity within *Tg* vacuoles could be reliably quantified using our artificial intelligence-based high-throughput image analysis workflow HRMAn (Fisch *et al*, 2019b) (**Figure 1A and Figure S1B**). These analyses revealed an increase in CellMask staining of PVs in IFNγ-primed THP-1 WT cells, indicating their disruption (**Figure S1B**). We next asked whether GBP1 contributed to *Tg* vacuole leakiness. Similar assays in IFNγ-primed THP-1 Δ*GBP1* cells showed that *Tg* vacuoles were not disrupted, as seen by the exclusion of CellMask dye (**Figure S1B**). Doxycycline induced re-expression of GBP1 (THP-1 Δ*GBP1*+Tet-*GBP1* cells) rescued vacuole breakage (**Figure S1B**); as control, empty vector transduced cells (THP-1 Δ*GBP1*+Tet-EV) behaved like *ΔGBP1* cells (**Figure S1B**). We used doxycycline-induced expression of mCherry-GBP1 (Fisch *et al*, 2019a) (THP-1 Δ*GBP1*+Tet-mCH-*GBP1* cells) to allow quantification of GBP1-recruitment to *Tg* and stratify data on whether PVs that were decorated with mCH-GBP1 lost their integrity. Indeed, a population of GBP1$^+$ PVs were unable to exclude CellMask dye clearly indicating loss of membrane integrity (**Figure 1A**). Taken together, we concluded that GBP1 is necessary for opening of *Tg* PVs and GBP1-targeted vacuoles preferentially undergo loss of membrane integrity.

As *Tg* infection activates AIM2, we wanted to visualise this process using single-cell assays. To this end, we labelled *Tg*-DNA with EdU by growing them in human foreskin fibroblasts (HFFs), whose DNA remains unlabelled as they do not replicate due to contact-dependent growth inhibition. Following infection of macrophages with EdU-labelled *Tg*, we visualised *Tg*-DNA with Alexa-647 fluorophore using click-chemistry and quantified macrophages containing cytosolic *Tg*-DNA (**Figure 1B**). Roughly 35% of infected macrophages contained *Tg*-DNA in their cytosol 6h p.i. and all cells displaying this phenotype had GBP1$^+$ PVs (**Figure 1B**). This showed that GBP1 targeting results in the release of *Tg*-DNA into host cell cytoplasm. We validated CellMask dye assays further by examining the ultrastructure of the vacuole membranes using correlative light-electron microscopy, which revealed ruffled and broken vacuole membranes in cells expressing GBP1 (**Figure 1C**). In THP-1 Δ*GBP1*, most PVs analysed by electron microscopy did not show structural defects or loss of membrane integrity (**Figure 1C**). Taken together, these results point towards an indispensable role for human GBP1 in the rupture of *Tg* PVs and release of microbial DNA into the cytosol.

We next wanted to address whether GBP1 contributed to phagocytosis of *Tg* in macrophages. Compartments containing phagocytosed *Tg* become RAB7$^+$ and the contained parasites are destroyed in lysosomes (Mordue & Sibley, 1997; Sugaya *et al*, 2011). WT and Δ*GBP1* THP-1 cells infected with *Tg* showed similar recruitment of endogenous RAB7 at 2 h post-infection (p.i.; **Figure 1D and Figure S2A**) which indicated that GBP1 does not contribute to *Tg* phagocytosis. By 6 hours p.i, *Tg* phagosomes had matured and cleared parasites, and only *Tg* that invaded and formed PVs remained (**Figure S2A**). To test if GBP1 was also recruited to phagosomes, we quantified the recruitment of mCH-GBP1 (Dox-treated Δ*GBP1*+Tet-mCH-*GBP1* cells) and endogenous RAB7 to *Tg* (**Figure 1E)**. This revealed an equal distribution of GBP1 on *Tg*-containing phagosomes (RAB7$^+$) and PVs (RAB7$^-$) at 2 hours p.i. (**Figure 1E**). At later time points, exclusively PVs remained, of which ~25% (type I *Tg*) to 35% (type II *Tg*) were decorated with GBP1 (**Figure 1E**). Thus, GBP1 targets both *Tg* phagosomes and PVs but does not contribute to *Tg* phagocytosis.

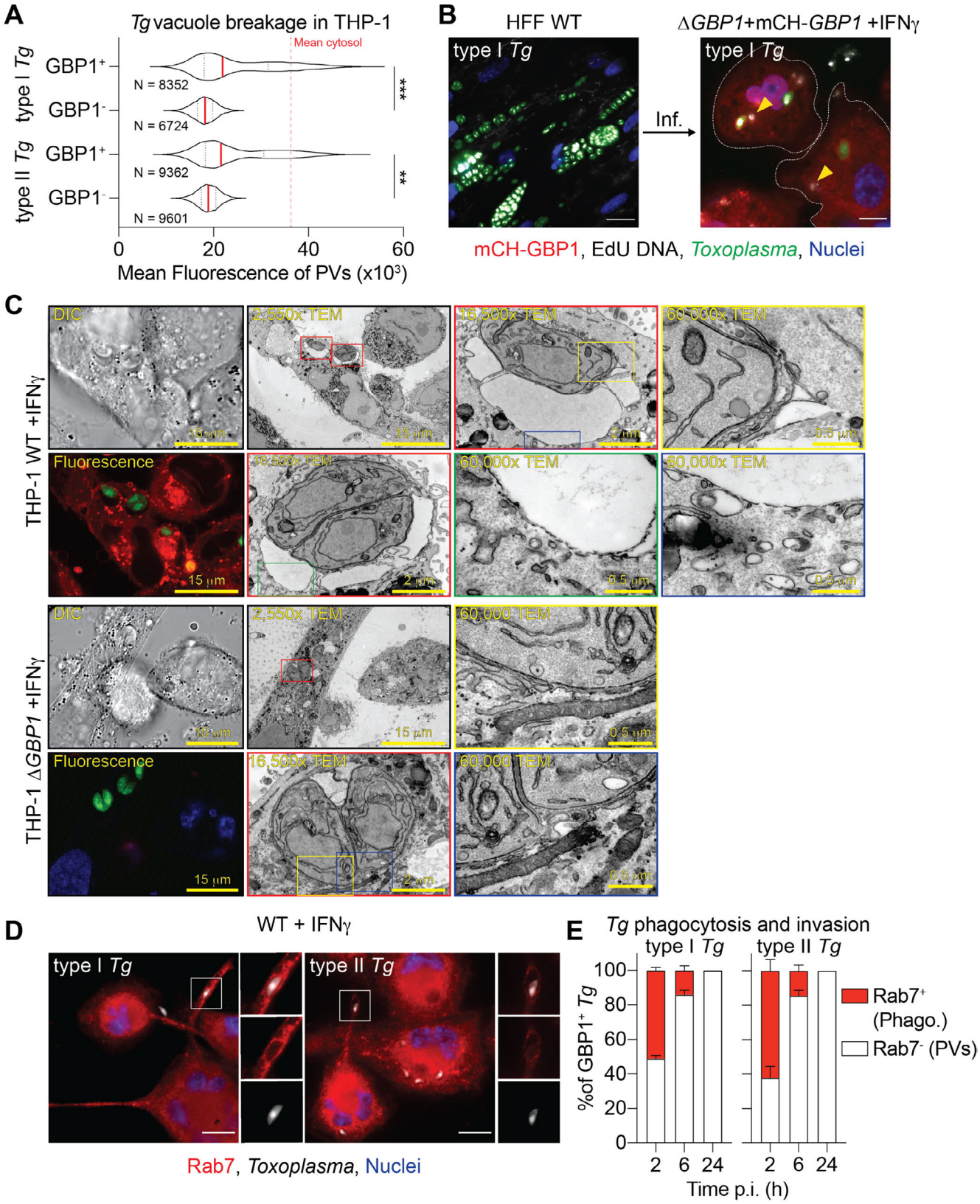

Does GBP1 contribute to growth-restriction of *Tg*? To addressed this, we performed plaque assays to enumerate live *Tg* after 18 h infection of THP-1 WT, Δ*GBP1* and Δ*GBP1*+Tet-*GBP1* reconstituted cells (**Figure S2B-D**). This revealed that IFNγ-stimulation of macrophages can control *Tg*-growth in a GBP1-dependent manner as we observed reduced plaque loss with parasites isolated from Δ*GBP1* cells (**Figure S2D**). Reconstitution of GBP1 by addition of Dox reversed the loss of restriction in *ΔGBP1* cells. Altogether, we concluded that GBP1 targets *Tg* PVs,

Figure 1: GBP1 disrupts *Toxoplasma* vacuoles leading to the release of parasite DNA into the macrophage cytosol.
(A) Representative quantification of CellMask fluorescence intensities within vacuoles (PV) of type I or type II *Toxoplasma gondii* (*Tg*) infected THP-1 Δ*GBP1*+Tet-mCH-*GBP1* pre-treated with IFNγ and Doxycycline (Dox) to induce GBP1 expression. Plotted depending on whether PVs were decorated with GBP1 (GBP1$^+$) or not (GBP1$^-$). Mean fluorescence signal of CellMask dye in the cytosol is indicated by dashed red line. N = number of vacuoles. **(B)** Left: Representative immunofluorescence image of type I *Tg* grown in human foreskin fibroblasts (HFF WT) in the presence of EdU DNA label. Labelled type I *Tg* were harvested from the HFFs and used to infect (Inf.) THP-1 Δ*GBP1*+Tet-mCH-*GBP1* for 6 hours. THP-1 cells were pre-treated with IFNγ and Dox to induce mCH-GBP1 expression (Right). Parasite DNA released into the cytoplasm was visualised by click-chemistry to label the incorporated EdU. Red: mCH-GBP1; White: EdU-DNA; Green: *Tg*; Blue: Nuclei. Cells are outlined by the white, dashed line and released *Tg*-DNA marked by yellow arrowheads. Scale bar 10 µm. **(C)** Representative images of correlative light and electron microscopy of THP-1 WT or Δ*GBP1* cells (flooded with CellMask for fluorescence imaging), pre-treated with IFNγ to induce GBP1 expression and infected with type I (RH) *Tg* for 6 hours. Parasites indicated within coloured boxes are shown at higher magnifications as indicated (DIC, differential interference contrast; TEM, transmission electron micrograph). Red: CellMask; Green: *Tg*; Blue: Nuclei. Scale bars as indicated. **(D)** Representative immunofluorescence images for the endogenous phagosome marker Rab7 in IFNγ-primed THP-1 WT cells infected with type I or type II *Tg* for 2 hours. Red: Rab7; Grey: *Tg*; Blue: Nuclei. Scale bar 15 µm. **(E)** Quantification of Rab7 and GBP1 recruitment to type I and type II *Tg* vacuoles and *Tg*-containing phagosomes (Phago.) in IFNγ and Dox treated THP-1 Δ*GBP1*+Tet-mCH-*GBP1*. Data are plotted as proportion of GBP1$^+$ parasites at indicated time post-infection. **Data information:** Graphs in **(A+E)** from n = 3 independent experiments. *P* values in **(A)** from nested t-test comparing GBP1$^+$ to GBP1$^-$ PVs following adjustment for multiple comparisons. ** *P ≤ 0.01 or* *** *P ≤ 0.001* in **(A)** for indicated comparisons of the means of the n = 3 independent experiments.

compromises their integrity and parasite viability and releases *Tg* DNA into the cytosol.

GBP1 does not participate in *Salmonella* vacuolar escape but targets cytosolic bacteria

Having established an indispensable role for GBP1 in opening of *Tg* PVs, we wanted to test if GBP1 also contributed to the escape of STm from *Salmonella*-containing vacuoles (SCVs). STm secretes effectors that disrupt endocytic trafficking and prevent fusion of degradative lysosomes with SCVs (Spanò & Galán, 2018). We therefore used differential permeabilization (Meunier & Broz, 2015) to determine whether the escape of STm from its vacuole into the cytosol required GBP1. Similar number of cytosolic STm were detected in WT and Δ*GBP1* cells, suggesting that GBP1 is dispensable for cytosolic escape of STm (**Figure 2A-B**). GBP1 recruits caspase-4 to STm and enhances pyroptosis (Fisch *et al*, 2019a). We performed quantitative immunofluorescence microscopy to determine spatiotemporal differences, if any, in GBP1 recruitment to bacteria over time (**Figure 2C**). Importantly, differential permeabilization revealed that GBP1 was exclusively recruited to cytosolic STm at all time points (**Figure 2D-E**). Studies in epithelial cells have shown that the lectin Galectin-8 (Gal-8) is recruited to disrupted SCVs, which promotes bacterial xenophagy and growth-restriction (Thurston *et al*, 2012). Consistent with a lack of a role for GBP1 in cytosolic escape of STm, similar proportions of STm were decorated with Gal-8 in WT and Δ*GBP1* cells (**Figure 2G**). Immunofluorescence microscopic staining of Gal-8 as a marker for disrupted SCVs further supported our finding that GBP1 is exclusively recruited to broken vacuoles (**Figure 2F-G**). Temporal studies showed that SCVs were rapidly disrupted (become Gal-8$^+$), but loose this marker over time (**Figure 2G**), as has been shown before in epithelial cells (Thurston *et al*, 2012). At later time points as the proportion of Gal-8$^+$ vacuoles decreased, cytosolic STm still retained GBP1 coating (**Figure 2G**). We therefore hypothesised that bacteria that lose Gal-8 marker become decorated with caspase-4. To assess this possibility, we determined whether Gal-8 and caspase-4 could be recruited to the same bacterium (**Figure 2H-I**). Remarkably, at 1 hour p.i. STm decorated with Gal-8 and GBP1 were also positive for caspase-4 (**Figure 2I**) indicating that the same intracellular STm can trigger xenophagy and pyroptosis pathways. Strikingly, at 2 hours p.i. a portion of cytosolic STm were positive for either GBP1-Gal-8 or GBP1-caspase-4 (**Figure 2I**). Over time the proportion of GBP1-Gal-8$^+$ bacteria decreased, which is consistent with increased GBP1-caspase-4-driven pyroptosis (**Figure 2I**). Altogether, these single-cell assays revealed that, unlike during *Tg* infection, GBP1 does not contribute to cytosolic escape of STm, but instead promotes the recruitment of caspase-4 to cytosolic STm, that have not been cleared by xenophagy, to enhance pyroptosis.

GBP1 facilitates formation of cytosolic signalling platforms

GBP1-mediated release of *Tg*-DNA or recruitment of caspase-4 to STm leads to execution of different cell death programs. GBP1 thus promotes the sensing of PAMPs and formation of cytosolic signalling platforms also known as supramolecular organizing centres (SMOCs) (Kagan *et al*, 2014). We investigated the structure of caspase activation SMOCs promoted by GBP1 actions using structured illumination microscopy (SIM). Upon *Tg* infection, AIM2 detects DNA and assembles ASC “specks”. Using SIM, we found that these atypical inflammasome complexes appear similar to previously described inflammasomes containing ASC and caspase-1 and caspase-8 (Man *et al*, 2013, 2014). We found a “donut”-like ASC ring enclosing caspase-8 in the centre (**Figure 3A-C and Figure S3A**). Furthermore, using THP-1 cells expressing myc-AIM2 (**Figure S3B**), we detected AIM2 recruitment to ASC specks in *Tg*-infected macrophages (**Figure 3B-C**). Similarly, in STm-infected macrophages, we found GBP1 recruited caspase-4 directly to the bacterial surface (**Figure 3D**). Bacteria were completely covered in GBP1, with a high degree of colocalisation with YFP-caspase-4^{C258S} (**Figure 3D**). These results clarify the distinct spatial roles of GBP1 during *Tg* and STm infection.

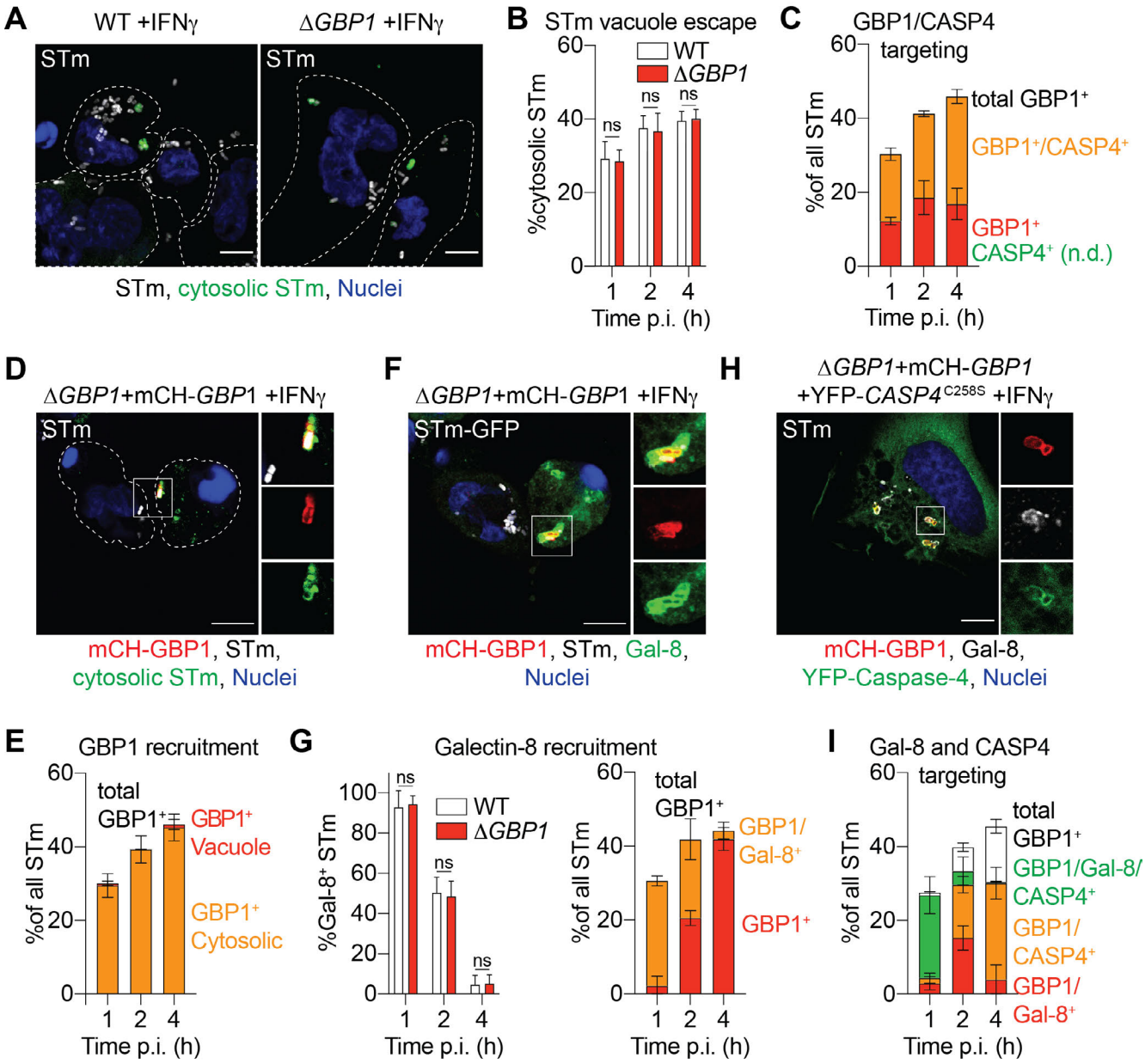

Figure 2: GBP1 only targets to cytosolic *Salmonella* to activate caspase-4
(A) Representative immunofluorescence images showing cytosolic *Salmonella* Typhimurium (STm) and all STm from differentially permeabilised, IFNγ-primed THP-1 WT or Δ*GBP1* cells infected with STm SL1344 (MOI = 30) for 2 hours. Cells are outlined by the white, dashed line. Grey: STm; Green: Cytosolic and extracellular STm; Blue: Nuclei. Scale bar 10 μm. **(B)** Quantification of the proportion of cytosolic STm SL1344 in differentially permeabilised and IFNγ-treated THP-1 WT or Δ*GBP1* at the indicated times post infection. **(C)** Quantification of GBP1 and caspase-4 (CASP4) recruitment to STm SL1344 in IFNγ and Doxycycline (Dox) treated THP-1 Δ*GBP1*+Tet-mCH-*GBP1*+YFP-*CASP4*^{C258S} at the indicated times post-infection. Percentage of all intracellular STm positive for the indicated markers is plotted. n.d. not detected. **(D)** Representative immunofluorescence images showing the recruitment of GBP1 to cytosolic STm. IFNγ-primed and Dox-treated THP-1 Δ*GBP1*+Tet-mCH-*GBP1* infected with STm SL1344 (MOI = 30) for 2 hours, differentially permeabilised and stained for cytosolic STm and total STm. Cells are outlined by the white, dashed line. Red: mCH-GBP1; Grey: STm; Green: Cytosolic STm; Blue: Nuclei. Scale bar 10 μm. **(E)** Quantification of GBP1 recruitment to cytosolic and intra-vacuolar STm SL1344 in differentially permeabilised and IFNγ and Dox treated THP-1 Δ*GBP1*+Tet-mCH-*GBP1* at the indicated times post infection (p.i.). **(F)** Representative immunofluorescence stain for galectin-8 (Gal-8) in IFNγ-primed and Dox-treated THP-1 Δ*GBP1*+Tet-mCH-*GBP1* infected with STm SL1344-GFP (MOI = 30) for 1 hour. Red: mCH-GBP1; Grey: STm; Green: Gal-8; Blue: Nuclei. Scale bar 10 μm. **(G)** Galectin-8 recruitment to STm is independent of GBP1 and reduces temporally during infection. **Left:** Quantification of Gal-8 recruitment to STm SL1344-GFP in IFNγ treated THP-1 WT or Δ*GBP1* at the indicated times post infection. **Right:** Quantification of Gal-8 recruitment to STm SL1344-GFP in IFNγ and Dox treated THP-1 Δ*GBP1*+Tet-mCH-*GBP1* at the indicated time post infection. **(H)** Representative immunofluorescence images showing galectin-8 (Gal-8) recruitment to STm in IFNγ-primed and Dox-treated THP-1 Δ*GBP1*+Tet-mCH-*GBP1*+YFP-*CASP4*^{C258S}. THP-1 cells were infected with STm SL1344 (MOI = 30) for 1 hour. Red: mCH-GBP1; Grey: Galectin-8; Green: YFP-caspase-4; Blue: Nuclei. Scale bar 10 μm. **(I)** Quantification of Gal-8 and caspase-4 (CASP4) recruitment to STm SL1344 in IFNγ and Dox treated THP-1 Δ*GBP1*+Tet-mCH-*GBP1*+YFP-*CASP4*^{C258S} at the indicated time post infection. **Data information:** Graphs in **(B, C, E, G, I)** show mean ± SEM from n = 3 independent experiments. *P* values for indicated comparisons in (**B**) and (**G**) from one-way ANOVA following adjustment for multiple comparisons. ns, not significant.

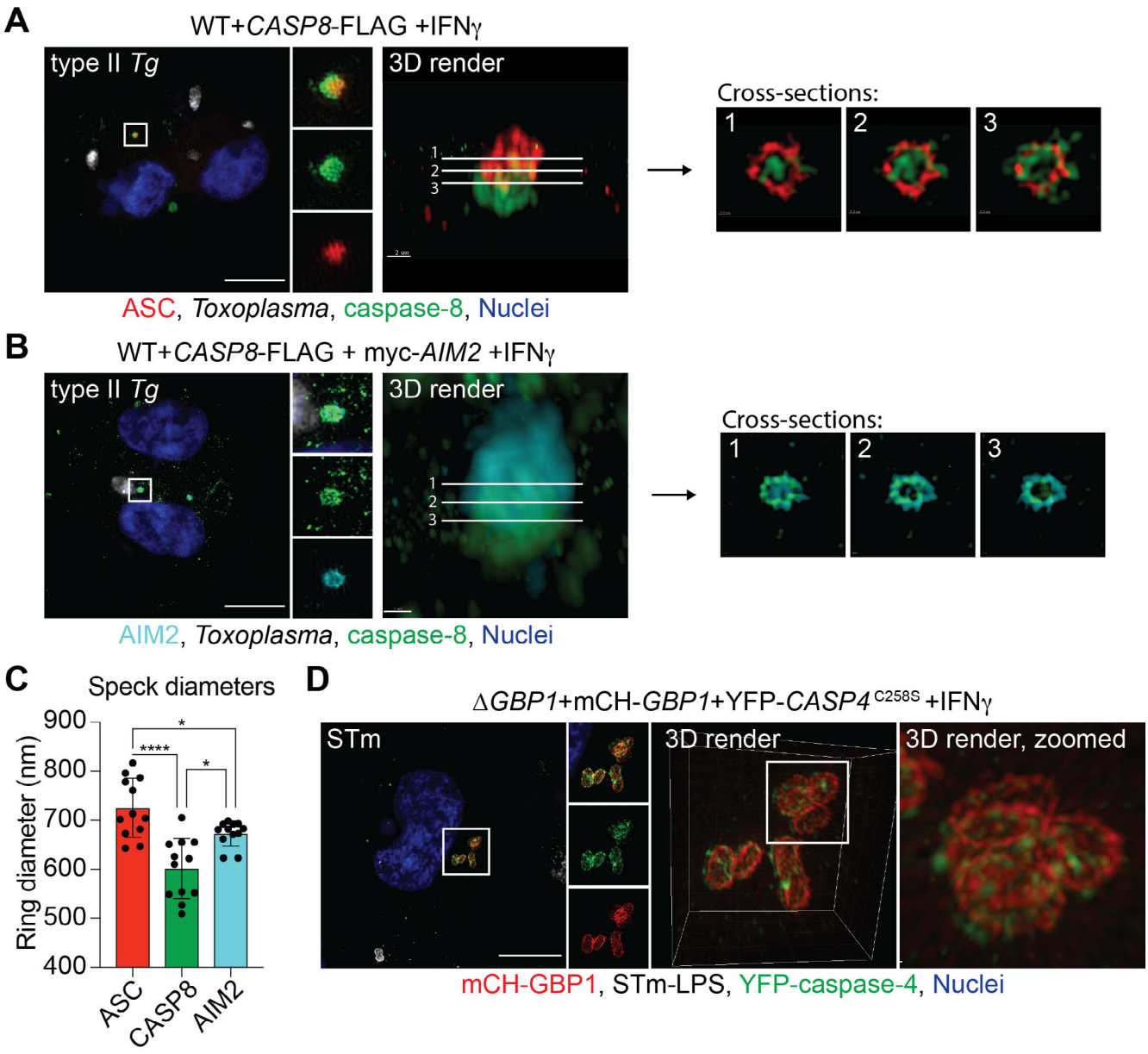

Figure 3: Macrophages form SMOCs downstream of GBP1 to control caspase activity
(A) Left: Representative structured illumination super-resolution immunofluorescence microscopy images from THP-1 WT+Tet-*CASP8*-FLAG cells treated with IFNγ and Doxycycline (Dox) to induce caspase-8 expression and then infected with type II *Toxoplasma gondii* (*Tg*) for 4 hours. **Right:** 3D reconstruction and slices through the ASC-caspase-8 speck seen in the image on the left. Red: ASC; Grey: *Tg*; Green: caspase-8; Blue: Nuclei. Scale bar 10 µm. **(B) Left:** Representative structured illumination super-resolution immunofluorescence microscopy images from THP-1+Tet-*CASP8*-FLAG+myc-*AIM2* cells treated with IFNγ and Dox and infected with type II *Tg* for 4 hours. **Right:** 3D reconstruction and slices through the AIM2-caspase-8 speck seen in the image on the left. Cyan: AIM2; Grey: *Tg*; Green: caspase-8; Blue: Nuclei. Scale bar 10 µm. **(C)** Ring diameters of the indicated proteins within an inflammasome speck from *Tg* infected cells shown in **(A)** and **(B)**. **(D) Left:** Representative structured illumination super-resolution immunofluorescence microscopy images from THP-1 Δ*GBP1*+Tet-mCH-*GBP1*+YFP-*CASP4*^{C258S} cell treated with IFNγ and Dox and infected with STm SL1344 (MOI = 30) for 2 hours. **Right:** 3D reconstruction of the GBP1-caspase-4 signalling platform on the cytosolic STm. Red: mCH-GBP1; Grey: STm-LPS; Green: YFP-caspase-4; Blue: Nuclei. Scale bar 10 µm. **Data information:** Graph in **(C)** shows quantification from n = 12 inflammasome specks and mean ± SEM. ** P ≤ 0.05; **** P ≤ 0.0001* for indicated comparisons in (**C**) from one-way ANOVA following adjustment for multiple comparisons.

GBP1 specifically promotes caspase-4 activation during STm infection

During STm infection, both caspase-1 and caspase-4 were found to contribute to pyroptosis based on whole-population assays such as LDH release or propidium iodide uptake assays (Fisch *et al*, 2019a). We asked whether both caspase-1 and caspase-4 were active in the same cell. Indeed, ~80 % STm-infected cells and cells that deposited GBP1 and caspase-4 on the bacteria also contained an ASC speck (**Figure 4A-B**). This was indicative of an active canonical inflammasome in response to other bacteria-derived PAMPs. Notably, caspase-4 was not recruited to ASC specks, which is consistent with previous work

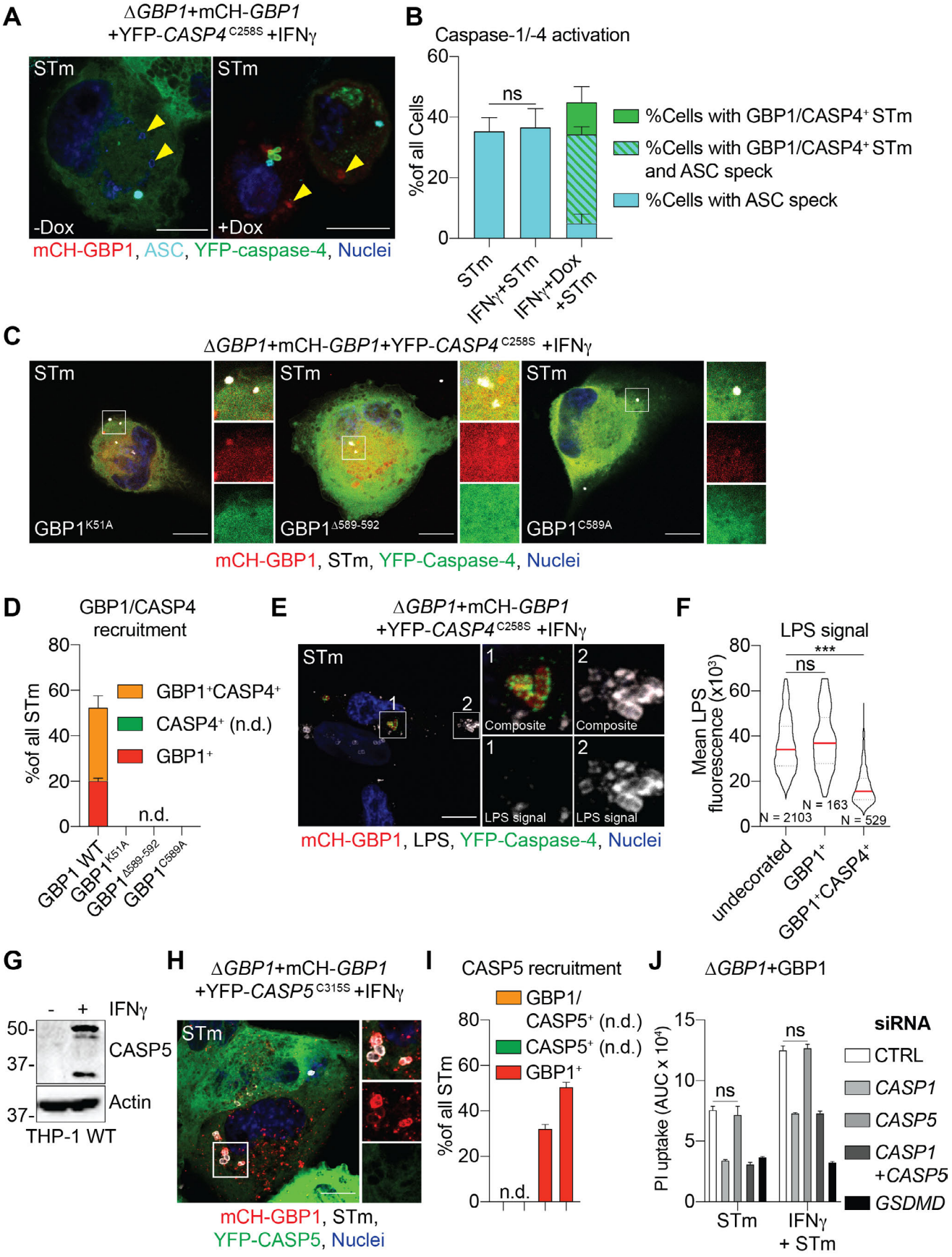

(Thurston *et al*, 2016) (**Figure 4A**). Active canonical inflammasomes were also found in STm-infected cells that lacked GBP1+ STm, but not in uninfected cells (**Figure 4B**). We therefore concluded that both caspase-1 and caspase-4 can be active in the same infected macrophage.

Figure 4: Selective caspase activation induces cell death in response to GBP1-mediated SMOC formation and *Salmonella* infection

(A) Representative immunofluorescence images from IFNγ-primed THP-1 Δ*GBP1*+Tet-mCH-*GBP1*+YFP-*CASP4*^{C258S} infected with *Salmonella* Typhimurium (STm) SL1344 (MOI = 30) for 2 hours stained for ASC. Cells were treated with Doxycycline (Dox) to induce GBP1 expression or left untreated. Yellow arrowheads indicate position of some STm within cells (DNA-staining dye). Red: mCH-GBP1; Cyan: ASC; Green: YFP-caspase-4; Blue: Nuclei. Scale bar 10 µm. **(B)** Quantification of ASC speck formation and GBP1+caspase-4 recruitment to STm at 2 h post-infection of THP-1 Δ*GBP1*+Tet-mCH-*GBP1*+YFP-*CASP4*^{C258S} cells left untreated of treated with IFNγ or IFNγ + Dox. **(C)** Representative immunofluorescence images from IFNγ-primed and Dox-treated THP-1 Δ*GBP1*+Tet-mCH-*GBP1*+YFP-*CASP4*^{C258S} cells infected with STm SL1344 (MOI = 30) for 2 hours. Cells expressed the indicated variants of GBP1: GBP1^{K51A} (lacking GTPase activity) or GBP1$^{\Delta589\text{-}592}$ or GBP1^{C589A}(which lack the isoprenylation site). Red: mCH-GBP1; Grey: STm; Green: YFP-caspase-4; Blue: Nuclei. Scale bar 10 µm. **(D)** Quantification of GBP1 and caspase-4 recruitment to STm SL1344 in IFNγ and Dox treated THP-1 Δ*GBP1*+Tet-mCH-*GBP1*+YFP-*CASP4*^{C258S} expressing the indicated version of GBP1 at 2 h post-infection. n.d. not detected. **(E)** Representative immunofluorescence images from IFNγ and Dox-treated THP-1 Δ*GBP1*+Tet-mCH-*GBP1*+YFP-*CASP4*^{C258S} cells infected with STm SL1344 (MOI = 30) for 2 hours and stained for STm LPS. Red: mCH-GBP1; Grey: STm-LPS; Green: YFP-caspase-4; Blue: Nuclei. Scale bar 10 µm. **(F)** Quantification of LPS immunofluorescence staining intensity from undecorated, GBP1^{+} or GBP1^{+}CASP4^{+} STm in the cytosol of infected THP-1 macrophages. **(G)** Caspase-5 expression is induced by IFNγ. Representative immunoblots for caspase-5 (CASP5) and β-actin of THP-1 WT treated with IFNγ as indicated. **(H)** Caspase-5 does not target STm. Representative immunofluorescence images from IFNγ-primed and Dox-treated THP-1 Δ*GBP1*+Tet-mCH-*GBP1*+YFP-*CASP5*^{C315S} infected with STm (MOI = 30) for 2 hours. Red: mCH-GBP1; Grey: STm; Green: YFP-caspase-5; Blue: Nuclei. Scale bar 10 µm. **(I)** Quantification of GBP1 and caspase-5 recruitment to STm in IFNγ and Dox treated THP-1 Δ*GBP1*+Tet-mCH-*GBP1*+YFP-*CASP5*^{C315S}. n.d. not detected. **(J)** Caspase-5 is dispensable for STm-induced pyroptosis. Real-time propidium iodide (PI) uptake assay from IFNγ-primed THP-1 Δ*GBP1* +Tet-*GBP1* cells transfected with indicated siRNA or non-targeting control (CTRL) infected with STm SL1344 (MOI = 30) for 4 h. Plotted as area under the curve (AUC) from real-time assays. **Data information:** Graph in **(B, D, F, I+J)** shows mean ± SEM of n = 3 independent experiments. *** $P \leq 0.001$ in **(F)** from nested one-way ANOVA comparing to undecorated vacuoles for the means of the n = 3 independent experiments and in (**B+J**) from two-way ANOVA following adjustment for multiple comparisons. ns, not significant.

We previously showed that the translocation of GBP1 to STm or *Tg* requires its GTPase function and isoprenylation (Fisch *et al*, 2019a). However, as GBP1 was dispensable for bacterial escape from SCVs, we wanted to examine whether lack of GBP1 targeting to STm also affected the recruitment of caspase-4 to bacteria. To address this, we expressed YFP-CASP4^{C258S} in THP-1 Δ*GBP1* cells reconstituted with doxycycline-inducible variants of GBP1 that lacked GTPase activity (GBP1^{K51A}) or isoprenylation sites (GBP1^{C589A} or GBP1$^{\Delta589\text{-}592}$; **Figure S3C**). None of these variants localised to STm nor did we observe recruitment of caspase-4 (**Figure 4C-D**). Along with above described findings on the lack of involvement of GBP1 in STm escape into the cytosol, these results indicated that the inability of GTPase or isoprenylation-deficient GBP1 in enhancing STm-induced pyroptosis was due to their inability to recruit and activate caspase-4 on the surface of cytosolic bacteria (Fisch *et al*, 2019a). Interestingly, immunofluorescence staining of *Salmonella*-LPS using a monoclonal antibody revealed that GBP1-CASP4^{+} bacteria stained not at all or poorly with anti-LPS, which suggested that access to the epitope might be blocked by the thick coat of GBP1 and caspase-4 on the bacterial surface. As LPS is a ligand for caspase-4, this finding is consistent with the possibility that caspase-4 on the bacterial surface precludes antibody-mediated staining of LPS (**Figure 4E-F**).

Caspase-5 is a human paralogue of caspase-4 and can also detect cytosolic LPS and trigger pyroptosis (Shi *et al*, 2014). We therefore wanted to assess its role during STm infection. Notably, caspase-5 expression was upregulated upon IFNγ treatment of macrophages (**Figure 4G**). However, unlike YFP-CASP4^{C258S}, YFP-*CASP5*^{C315S} was not recruited to STm (**Figure S3D, 4H-I**). Notably, STm that were negative for caspase-4 but positive for GBP1 could be stained with the anti-LPS antibody (**Figure 4H**), which suggested that caspase-4 is responsible for the reduced antibody access. Silencing of caspase-5 expression did not affect pyroptosis in STm-infected IFNγ-primed macrophages (**Figure 4J, S3E**), which further pointed to a unique role for caspase-4 in this scenario. These experiments together established that both caspase-1 and caspase-4 are active within the same cell and GBP1 controls caspase-4 recruitment and activation directly on the surface of cytosolic bacteria, whereas caspase-5 is dispensable for STm-induced pyroptosis.

Caspase-1 controls GBP1-mediated pyroptosis through negative feedback

Caspase-1 can cleave GBP1 at Asp192 to generate a stable p47 GBP1 C-terminal fragment in human umbilical vein endothelial cells (HUVECs) (Naschberger *et al*, 2017). However, the impact of this proteolytic event on GBP1 function during infections has not been examined. To study this further, we created THP-1 Δ*GBP1* cells expressing the non-cleavable GBP1^{D192E} without or with an mCherry tag (THP-1 Δ*GBP1*+Tet-*GBP1*^{D192E} and THP-1 Δ*GBP1*+Tet-mCH-*GBP1*^{D192E} cells; **Figure S4A**). Aspartate D192 is in a surface-exposed loop within the GTPase domain of GBP1 (Prakash *et al*, 2000) and therefore likely to be accessible to proteases (**Figure S4B**). Immunoblotting for GBP1 from STm-infected IFNγ-primed macrophages revealed caspase-1 activation and formation of p47 GBP1 from cells expressing wildtype GBP1 but not GBP1^{D192E} (**Figure 5A**). Furthermore, silencing caspase-1, but not caspase-4, abolished p47 GBP1 production (**Figure 5B**), which suggested that caspase-1 plays a dominant role in GBP1 proteolysis. Similarly, chemical activation of caspase-1 by treatment with LPS+Nigericin produced a p47 GBP1 fragment (**Figure 5B**). To investigate whether trafficking of GBP1^{D192E} is altered, we infected the mCH-GBP1^{D192E} expressing cells with

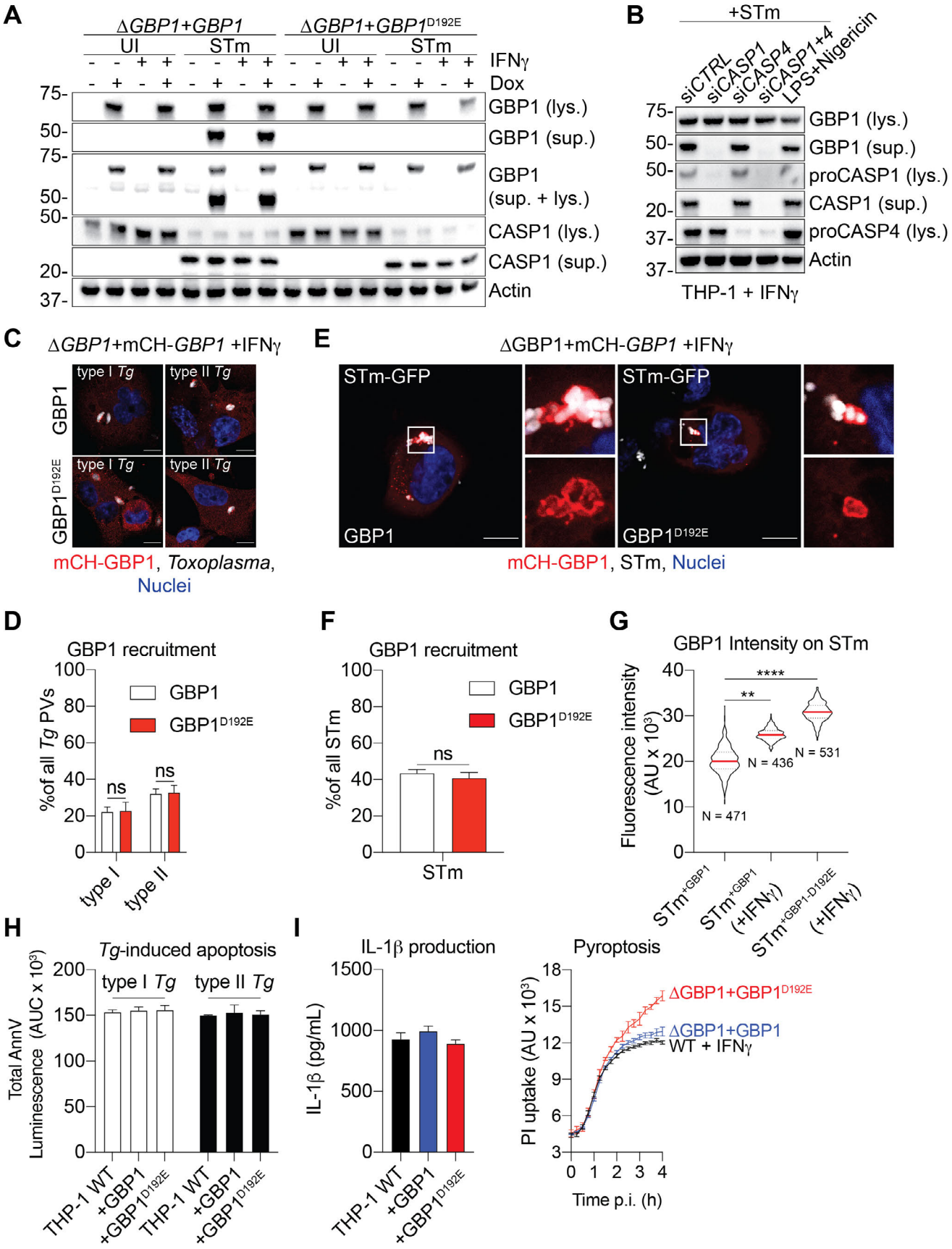

Tg or STm and quantified GBP1 recruitment to PVs or cytosolic STm respectively. Upon infection with *Tg* we did not observe differences in the proportion of *Tg*-PVs (**Figure 5C-D**) or STm (**Figure 5E-F**) that became GBP1-positive, which indicated that proteolysis of GBP1 is dispensable for its trafficking to microbial

Figure 5: Caspase-1, caspase-4 and GBP1 act in a feedback loop to control cell death and IL-1β secretion of *Salmonella*-infected macrophages
(A) GBP1, but not GBP1^{D192E}, is cleaved during STm infection. Representative immunoblots for GBP1, caspase-1 (CASP1) and β-actin from lysates (lys.) or culture supernatants (sup.) of THP-1 Δ*GBP1*+Tet-*GBP1* WT or D192E cells treated with IFNγ and Dox as indicated and infected with STm SL1344 for 4 hours or left uninfected (UI). **(B)** Caspase-1 is required for GBP1 cleavage. Representative immunoblots for GBP1, caspase-1 (CASP1), caspase-4 (CASP4) and β-actin from lysates (lys.) or culture supernatants (sup.) of THP-1 WT, transfected with the indicated siRNA and infected with STm SL1344 for 4 hours or treated with LPS and Nigericin for 90 minutes. **(C)** Representative immunofluorescence images from IFNγ-primed and Doxycycline (Dox)-treated THP-1 Δ*GBP1*+Tet-mCH-*GBP1* or mCH-*GBP1*^{D192E} cells infected with type I or type II *Toxoplasma gondii* (*Tg*) for 6 hours. Red: mCH-GBP1; Grey: *Tg*; Blue: Nuclei. Scale bar 10 µm. **(D)** Quantification of recruitment of GBP1 WT or GBP1^{D192E} to type I or type II *Tg* at 6 hours post infection in THP-1 cells pre-stimulated with IFNγ and Dox to induce GBP1 expression. **(E)** Representative immunofluorescence images from IFNγ-primed and Dox-treated THP-1 Δ*GBP1*+Tet-mCH-*GBP1* or mCH-*GBP1*^{D192E} cells infected with STm SL1344-GFP (MOI = 30) for 2 hours. Red: mCH-GBP1; Grey: STm; Blue: Nuclei. Scale bar 10 µm. **(F)** Quantification of recruitment of GBP1 WT or GBP1^{D192E} at 4 hours post-infection with STm SL1344-GFP in THP-1 cells pre-stimulated with IFNγ and Dox to induce GBP1 expression. **(G)** Representative fluorescence intensities of the indicated GBP1 variants on the surface of decorated STm SL1344-GFP in THP-1 cells 4 hours post-infection. N depicts the number of measured GBP1^{+} bacteria in the respective condition. **(H)** GBP1^{D192E} and WT GBP1 behave similarly in *Tg*-induced atypical apoptosis. AnnV-Glo assay of THP-1 WT and Δ*GBP1* cells stably reconstituted with Tet-*GBP1* WT or *GBP1*^{D192E} mutant as indicated, infected with type I or type II *Tg* for 18 h. Plotted as area under the curve (AUC) from real-time assays. **(I)** GBP1^{D192E} promotes increased pyroptosis during STm-infection. **Left:** IL-1β ELISA from the indicated THP-1 cells primed with IFNγ and Dox infected with STm SL1344 (MOI = 30) at 4 h post-infection. **Right:** Real-time propidium iodide (PI) uptake assay from IFNγ-primed THP-1 cells of the indicated genotypes and infected with STm SL1344 for 4 h. **Data information:** Graphs in **(D, F, G, H, I)** show mean ± SEM from n = 3 independent experiments. ** *P* ≤ *0.01,* *** *P* ≤ *0.001* **** *P* ≤ *0.0001* for indicated comparisons in **(G)** from nested one-way ANOVA comparing means of the n = 3 experiments and in **(D, F)** from two-way ANOVA following adjustment for multiple comparisons; ns, not significant.

vacuoles. However, the mean fluorescence intensity of mCH-GBP1 around decorated STm was markedly higher in cells expressing the GBP1^{D192E} variant (**Figure 5G**), even though the expression of wildtype GBP1 and GBP1^{D192E} were comparable (**Figure S4C-D**). We speculated that cleavage of GBP1 may reduce the cellular pool of full-length GBP1, which would also reduce its ability to induce cell death over time. We therefore compared apoptosis and pyroptosis in GBP1 and GBP1^{D192E} expressing cells. Apoptosis induced by *Tg* infection of THP-1 macrophages expressing GBP1 or GBP1^{D192E} variant were similar, and we reasoned that this is because *Tg*-infection does not involve activate caspase-1 (**Figure 5H**). However, during STm infection, GBP1^{D192E} cells underwent higher pyroptosis but released similar levels of IL-1β (**Figure 5I**). This finding is consistent with a major role for GBP1 in promoting caspase-4-driven pyroptosis, but not canonical caspase-1 activation, which is responsible for IL-1β production (**Figure 5I**). Taken together, these results suggested that active caspase-1 cleaves GBP1 into an p47 fragment that reduces its recruitment to STm and the recruitment and activation of caspase-4. Because IL-1β maturation was not affected by GBP1^{D192E} mutation, we speculate that this caspase-1-driven feedback mechanism balances cell death and IL-1β secretion during STm infection. Moreover, as caspase-1 does not contribute to cell death during *Tg*-infection, this feedback regulatory mechanism is pathogen-specific.

DISCUSSION

IFNγ-inducible GBPs have emerged as important proteins in host defence against a range of pathogens. However, GBPs probably play differential and hence nuanced roles in host defence against different pathogens and these differences remain largely unexplored. Additionally, besides direct attack on pathogens and release of PAMPs, other true mechanistic contribution of GBPs to processes of pathogen restriction and host cell death induction are still lacking. Our studies provide new mechanistic insights on the role of human GBP1 in macrophages infected with two evolutionarily divergent pathogens.
We established that GBP1 controlled the fitness of *Tg* in infected macrophages and promotes lysis of *Tg*-containing vacuoles, release of *Tg*-DNA and assembly of the AIM2-ASC-caspase-8 SMOC that induces apoptosis. *Tg* viability in infected macrophages is reduced through the actions of GBP1. Thus, GBP1 not only removes a replicative niche through apoptotic killing of macrophages, but also controls parasite growth. Unfortunately, due to high levels of pyroptotic loss of macrophages, we could not accurately determine the fate of GBP1-targeted bacteria using gentamicin-protection assays (Miao *et al*, 2010).

Results obtained are consistent with similar GBP1 recruitment to *Tg*-containing vacuoles and phagosomes (Qin *et al*, 2017; Shydlovskyi *et al*, 2017; Fisch *et al*, 2019a). Our single-cell assays conclusively reveal that GBP1 decorates two distinct intracellular populations of *Tg* within the same cell – those formed by host-mediated phagocytosis or those formed by *Tg* invasion. These compartments are of different origin and have different membrane compositions. GBP1 is recruited to *Tg* only in IFNγ-primed macrophages, suggesting that other IFNγ-inducible factors also contribute to GBP1 trafficking. In addition, we have previously shown that GBP1 GTPase activity and isoprenylation control its trafficking to *Tg* (Fisch *et al*, 2019a). Therefore, GBP1-intrinsic and extrinsic activities control its ability to target *Tg,* which need to be investigated in the future.

GBP1 targeting of *Tg* vacuolar membranes was required for their compromise and release of *Tg*-DNA, which resembled bacterial lysis in the cytosol by murine GBPs (Man *et al*, 2015; Meunier *et al*, 2015; Liu *et al*, 2018). In contrast, STm enters the cytosol independently of GBP1. This yet again indicates that the actions of GBP1 are microbe-specific. GBP1 is a

dynamin-like GTPase and thus it may actively alter biological membranes (Huang *et al*, 2019). Recombinant, farnesylated GBP1 has been shown to bend lipids in the form of giant unilamellar structures *in vitro* (Shydlovskyi *et al*, 2017). Membrane disruption has been demonstrated for murine Gbps, as several Gbp family members are responsible for the formation of membrane blebs on *Tg* vacuoles (Yamamoto *et al*, 2012; Degrandi *et al*, 2013; Selleck *et al*, 2013; Kravets *et al*, 2016). Results from our correlative light and electron microscopy experiments reveal a similar phenotype, which is GBP1-dependent, in human macrophages. This is the first direct demonstration of a human GBP being capable of disrupting pathogen vacuole membranes. Importantly, using *Tg,* whose DNA was specifically labelled with EdU, we conclusively show the release of *Tg*-DNA into the host cytosol for detection by AIM2. Thus, during *Tg* infection GBP1 acts upstream of cell death execution and facilitates AIM2 signalling.

As caspase-1 and several other inflammasome-associated proteins are absent in *Tg*-infected cells, AIM2 recruits ASC and caspase-8 (Fisch *et al*, 2019a). The structure of a caspase-8 containing AIM2 inflammasome, imaged with super-resolution fluorescence microscopy, closely resembles previously published structures of caspase-8 in NLRP3/NLRC4 inflammasomes (Man *et al*, 2014, 2013). These appear as typical ASC donut-like rings with AIM2 on the inside and caspase-8 in the centre. ASC and AIM2 seem to form a dome under which caspase-8 can oligomerize and self-activate. This resembles death receptor-induced signalling complexes (DISCs)-driven caspase-8 activation during extrinsic apoptosis (Tummers & Green, 2017). It will be interesting to investigate whether the caspase-8 inhibitor c-FLIP (*CFLAR*) or FADD are recruited to this complex to moderate caspase-8 activity (Wu *et al*, 2014).

The role of GBP1 during STm infection is to directly recruit caspase-4 to the outer surface of bacteria for LPS-sensing and subsequent pyroptosis. Notably, GBP1 exclusively targeted cytosolic STm and did not contribute to their vacuolar escape. Equally, GBP1 detection of cytosolic STm was independent of recruitment of Gal-8, which belongs to a family of lectins that can detect vacuole rupture when luminal polysaccharides become exposed to the cytoplasm (Coers, 2017). Both GBP1 and Gal-8 were recruited to bacteria early during infection, and it has been suggested that GBP1 can bind endogenous sulphated lipids exposed to the cytoplasm (Bradfield, 2016). Importantly, GBP1 GTPase activity and isoprenylation were essential for GBP1-targeting to STm and subsequent recruitment of caspase-4, pointing further to GBP1-intrinsic and -extrinsic factors in regulating GBP1 trafficking. As STm infection progresses, GBP1-caspase-4 dual recruitment increases, and the proportion of Gal-8-positive bacteria is reduced over time. In epithelial cells, Gal-8 is rapidly recruited to cytosolic STm leading to bacterial xenophagy, during which Gal-8 is lost from bacteria over time (Thurston *et al*, 2012). In macrophages, we find that GBP1 is present on cytosolic STm even though they have lost the Gal-8 coat. Our findings on GBP1-independent recruitment of Gal-8 to STm are consistent with work with murine GBPs, where galectins-3 and -8 were needed for mGBP recruitment to Gram-negative bacteria (Feeley *et al*, 2017). We speculate that the cells first try to control the contamination of the cytosol with autophagic bacteria-clearance, but if this fails use GBP1 to induce the more drastic control measure to execute pyroptosis via caspase-4.

GBP1 and caspase-4 formed a dense coat on STm, which reduced bacterial staining with anti-LPS antibody. Whether this was due to reduced antibody access due to the GBP1/caspase-4 coat or blocking of the LPS epitope by caspase-4 cannot be definitively distinguished. As caspase-4 by itself could not recruit to the bacteria, we can hypothesise that GBP1 is involved in exposing parts of the LPS that are buried deeper within the membrane. Data derived from *Francisella* LPS suggests that tetra-acylated lipid A is recognized by caspase-4, but not murine caspase-11 (Lagrange *et al*, 2018) and we can therefore assume that GBP1 'opens' the bacterial outer membrane for caspase-4 to gain access to otherwise hidden PAMPs. Interestingly, caspase-5 was not recruited to STm even though previous work has shown that caspase-5 can bind LPS and promote pyroptosis in response to LPS transfection (Shi *et al*, 2014). These differences between caspase-4 and caspase-5 were unexpected and suggest that like the GBPs, even very similar members of the family members of human caspases have unique roles during infection. In naïve macrophages, the STm SPI2 virulence system, which is expressed late during infection, can subvert NLRP3 and NLRC4 inflammasomes and both caspase-4 and caspase-5 contribute to late pyroptosis (Baker *et al*, 2015; Bierschenk *et al*, 2019). As IFNγ-priming results in rapid recruitment of GBP1 and caspase-4 to STm and increased pyroptosis, it is plausible that the late role of caspase-5 in STm-induced cell death in naïve cells is not observed in our experimental conditions.

Taken together, during *Tg* infection GBP1 releases PAMPs that trigger SMOC formation and during STm infection GBP1 is a part of the SMOC itself. Given the upstream role of GBP1 in cell death, we hypothesised that GBP1 must be part of a regulatory feedback loop to limit its own activity. We found that canonical caspase-1 activation during STm infection, which is absent during *Tg* infection, limits caspase-4-driven pyroptosis by cleavage of GBP1 at D192. We thus show for the first time that GBP1 proteolysis directly regulates host cell death levels during infection. As caspase-4 does not contribute to IL-1β processing during STm infection, this regulatory feedback does not affect IL-1β production, which is largely driven by the canonical caspase-1 activation pathway. This tightly controlled mechanism is an example of the influence of cell death induction and execution mechanisms

controlling not only themselves, but also the amount of inflammation and tissue damage they cause. This contrasts our discovery of the ubiquitin conjugating enzyme UBE2L3 as an indirect target of caspase-1 that specifically control IL-1β production, but not pyroptosis (Eldridge *et al*, 2017). Studies on cellular targets of caspases may therefore provide new insights on homeostasis and disease (Sanchez-Garrido *et al*, 2018).

On a whole-organism level, fine tuning inflammation through IL-1β production or pyroptotic cell death is essential to contribute to a balanced immune response. Overall, our studies highlight the GBP1-mediated molecular mechanisms and functions of cell death regulation during infection with evolutionary different microbes.

AUTHOR CONTRIBUTION

DF, ARS and EMF conceived the idea for the study, DF, BC, MCD and TM performed experiments. HB, MY provided essential reagents. LMC provided essential expertise and equipment. DF, ARS and EMF analyzed and interpreted the data and wrote the manuscript. All authors revised the manuscript.

CONFLICT OF INTEREST

The authors declare that they have no conflict of interest.

ACKNOWLEDGEMENTS

We would like to thank Matt Renshaw for help with super-resolution SIM imaging, Julia Sanchez-Garrido for help in optimizing immunoblots and advice on reagents, the Crick High-throughput screening (HTS) STP for help in performing automated imaging experiments, the Crick Genomics and Equipment Park STP for performing sequencing and DNA minipreps for cloning. We thank all members of the Frickel and the Shenoy labs for productive discussion and Crick Core facilities for assistance in the project.

FUNDING

This work was supported by the Francis Crick Institute, which receives its core funding from Cancer Research UK (FC001076 to EMF, FC001999 to LMC), the UK Medical Research Council (FC001076 to EMF, FC001999 to LMC), and the Wellcome Trust (FC001076 to EMF, FC001999 to LMC). EMF was supported by a Wellcome Trust Career Development Fellowship (091664/B/10/Z). DF was supported by a Boehringer Ingelheim Fonds PhD fellowship. ARS would like to acknowledge support from the MRC (MR/P022138/1) and Wellcome Trust (108246/Z/15/Z). MY was supported by the Research Program on Emerging and Re-emerging Infectious Diseases (JP18fk0108047) and Japanese Initiative for Progress of Research on Infectious Diseases for global Epidemic (JP18fk0108046) from Agency for Medical Research and Development (AMED). HB was supported by Grant-in-Aid for Scientific Research on Innovative Areas (17K15677) from Ministry of Education, Culture, Sports, Science and Technology.

MATERIALS AND METHODS

Cells and parasites

THP-1 (TIB-202, ATCC) were maintained in RPMI with GlutaMAX (Gibco) supplemented with 10% heat-inactivated FBS (Sigma), at 37˚C in 5% CO_2 atmosphere. THP-1 cells were differentiated with 50 ng/mL phorbol 12-myristate 13-acetate (PMA, P1585, Sigma) for 3 days followed by a rested for 2 days in complete medium without PMA. Cells were not used beyond passage 20. HEK293T and human foreskin fibroblasts (HFF) were maintained in DMEM with GlutaMAX (Gibco) supplemented with 10% FBS at 37˚C in 5% CO_2 atmosphere. An overview of all cell lines made/ used in this study is provided in **Table 1**. *Tg* expressing luciferase/eGFP (RH type I and Prugniaud (Pru) type II) were maintained by serial passage on monolayers of HFF cells. All cell culture was performed without addition of antibiotics unless otherwise indicated. Cell lines were routinely tested for mycoplasma contamination by PCR and agar test.

Cell treatments

Cells were stimulated for 16 h prior to infection in complete medium at 37˚C with addition of 50 IU/mL human IFNγ (285-IF, R&D Systems). Induction of GBP1 or caspase-8 expression in the Doxycycline-inducible cells was performed with 200 ng/mL Doxycycline overnight (D9891, Sigma). To chemically activate caspase-1, cells were treated with 10 µM Nigericin (N1495, Invitrogen) and 100 µg/mL LPS-*Sm* (IAX-100-011, Adipogen).

Toxoplasma gondii infection

Parasite were passaged the day before infection. *Tg* tachyzoites were harvested from HFFs by scraping and syringe lysing the cells through a 25 G needle. The *Tg* suspension was cleared by centrifugation at 50 x g for 5 min and then the parasites were pelleted by centrifugation at 550 x g for 7 min from the supernatant, washed with complete medium, centrifuged again and finally re-suspended in fresh medium. Viable parasites were counted with trypan blue and used for infection at a multiplicity of infection (MOI) of 3 for most experiments or 1 for immunofluorescence imaging. Infection was synchronized by centrifugation at 500 x g for 5 min. Two hours after infection, extracellular parasites were removed with three PBS washes.

Plaque assay and quantification

To quantify *Tg* fitness following infection of macrophages, differentiated THP-1 cells were infected with *Tg* as described above and 18 hours p.i. supernatant and cells were harvested from the wells of a 12-well plate. Cells were syringe-lysed and obtained parasites from within the cells and the supernatant were diluted 1:10,000 and added to HFFs grown confluent in

wells of a 24-well plate. 5 days post infection of the HFFs, cells were fixed with ice-cold methanol and stained with crystal violet. Following 5 washes with PBS, plaques were imaged on a GelCount™ Colony Counter (Oxford Optronix) and cell covered area determined using FIJI ImageJ. Proportion of plaque and plaque loss as compared to *Tg* grown in untreated THP-1 were calculated subsequently.

***Salmonella* Typhimurium infection**

STm strain SL1344-GFP (with pFPV25.1 plasmid) was maintained under Ampicillin selection (11593027, Gibco) and grown on LB + Ampicillin agar plates. STm SL1344 wildtype strain was maintained in the presence of streptomycin (11860038, Gibco) selection. One day before infection bacteria from a single colony were inoculated into 9 mL LB and grown overnight at 37°C. The overnight culture was diluted 1:50 into LB + 300 mM NaCl (746398, Sigma) and grown shaking in a closed container until an OD_{600} of 0.9. Bacteria were harvested by centrifugation at 1000 x g for 5 min and washed with serum-free cell culture medium twice and re-suspended in 1 mL medium. Cells were infected with STm at an MOI of 30 and infections were synchronized by centrifugation at 750 x g for 10 min. Infected cells were washed 30 min post-infection three times with warm PBS (806552, Sigma) to remove extracellular bacteria and fresh medium containing 100 µg/mL Gentamicin (15750060, Gibco) was added for 1 h. Medium was then replaced with medium containing 10 µg/mL gentamicin and the infection continued for indicated times. Bacterial MOI used for infections were confirmed by plating on LB agar plates.

Real-time propidium iodide (PI)-uptake assays

To measure live kinetics of cell death, 60,000 cells were seeded per well of a black-wall, clear-bottom 96-well plate (Corning) for differentiation with PMA, treated and infected as described above. Medium was replaced with phenol-red-free RPMI supplemented with 5 µg/mL propidium iodide (P3566, Invitrogen). The plate was sealed with a clear, adhesive optical plate seal (Applied Biosystems) and placed in a plate reader (Fluostar Omega, BMG Labtech) pre-heated to 37°C. PI fluorescence was recorded with top optics every 15 min for times as indicated.

AnnV glow assay

Apoptosis kinetics were analyzed using the RealTime-Glo™ Annexin V Apoptosis Assay (JA1001, Promega) according to the manufacturer's instruction. 60,000 cells were seeded per well of a white, tissue culture-treated 96-well plate, differentiated, pre-treated and infected as described before. Simultaneously with infection, detection reagent was added. Luminescence was measured using a Fluostar Omega plate reader (BMG Labtech). No-cell, medium-only controls were used for background correction.

IL-1β ELISA

The cell culture supernatant was harvested and cleared by centrifugation at 2000 x g for 5 minutes. Cleared supernatants were then diluted in the buffer provided with the ELISA kit and ELISA was performed according to the manufacturer's instruction. IL-1β ELISA kit was from Invitrogen (#88-7261, detection range 2 - 150 pg/mL).

Immunoblotting

For immunoblotting, $0.5x10^6$ cells were seeded per well of a 48-well plate, differentiated with PMA, pre-treated and infected. At the end of treatments, cells were washed with ice-cold PBS and lysed for 5 min on ice in 50 µL RIPA buffer supplemented with protease inhibitors (Protease Inhibitor Cocktail set III, EDTA free, Merck) and phosphatase inhibitors (PhosSTOP, Roche). Lysates were cleared by centrifugation at full speed for 15 min at 4°C. BCA assay (Pierce BCA protein assay kit, 23225, Thermo Scientific) was performed to determine protein concentration. 10 µg of total protein per sample were run on 4-12% Bis-Tris gels (Novex, Invitrogen) in MOPS running buffer and transferred on Nitrocellulose membranes using iBlot transfer system (Invitrogen). Depending on the primary antibody used the membranes were blocked with either 5% BSA (A2058, Sigma) or 5% dry-milk (M7409, Sigma) in TBS-T for at least 1 h at room temperature. Incubation with primary antibodies was performed at 4°C overnight (all antibodies used in this study can be found in **Table 2**). Blots were developed by washing the membranes with TBS-T, probed with 1:5000 diluted secondary antibodies in 5% BSA in TBS-T and washed again. Finally, the membranes were incubated for 2 minutes with ECL (Immobilon Western, WBKLS0500, Millipore) and luminescence was recorded on a ChemiDoc MP imaging system (Biorad).

For immunoblots of culture supernatants, cells were treated in OptiMEM (1105802, Gibco) without serum. Proteins in the supernatants were precipitated with 4x volume cold acetone (V800023, Sigma) overnight at -20°C, and pelleted by centrifugation. Pellets were air dried and re-suspended in 40 µL 2x Laemmli loading dye.

Quantitative RT-PCR (qRT-PCR)

RNA was extracted from $0.25x10^6$ cells using Trizol reagent (15596026, Invitrogen). RNA (1 µg) was reverse transcribed using high-capacity cDNA synthesis kit (4368813, Applied Biosystems). qPCR used PowerUP SYBR green (A25742, Applied Biosystems) kit, 20 ng cDNA in a 20 µL reaction and primers (CASP5-fwd: 5'-GCAAGGAATGGGGCTCACTA-3'; CASP5-rev: 5'-CGTGCTGTCAGAGGACTTGT-3') at 1 µM final concentration on a QuantStudio 12K Flex Real-Time PCR System (Applied Biosystems). Recorded C_t values were normalized to C_t of human *HPRT1* (see Fisch et al, 2019a) and data plotted as ΔC_t (Relative expression).

siRNA transfection

Cells were transfected with siRNAs two days prior to infection, at the same time the THP-1 differentiation medium was replaced with medium without PMA. All siRNAs were used at a final concentration of 30 nM. For transfection, a 10x mix was prepared in OptiMEM containing siRNA(s) and TransIT-X2 transfection reagent (MIR 600x, Mirus) in a 1:2 stoichiometry. All siRNAs used in this study were OnTarget Plus smart pool siRNAs (Dharmacon):

Gene	Cat. number	Gene	Cat. number
CASP1	L-004401	*GSDMD*	L-016207
CASP4	L-004404	Neg. CTRL	D-001810
CASP5	L-004405		

Creation of new cell lines

Creation of the Dox-inducible GBP1 and caspase-8 cell lines

THP-1 Δ*GBP1*+Tet-*GBP1* and THP-1 Δ*GBP1*+Tet-mCH-*GBP1* have been published before and the THP-1 WT+Tet-CASP8-FLAG cells were created identically using Lentiviral transductions (Fisch *et al*, 2019a).

To create the caspase-8-3xFLAG expressing Dox-inducible plasmid (pLenti-Tet-*CASP8*-3xFLAG), the empty vector backbone was digested with BamHI, *CASP8* ORF was amplified from pcDNA3-*CASP8* by PCR (Addgene #11817, a gift from Guy Salvesen) (Stennicke & Salvesen, 1997), 3xFLAG was amplified from lentiCRISPRv2 (Addgene #52961, a gift from Feng Zhang) (Sanjana *et al*, 2014) and all fragments assembled with a Gibson assembly. All primers used for cloning PCRs can be found in **Table 3**.

To make the cells expressing GBP1^{D192E}, the pLenti-Tet-mCH-GBP1 and pLenti-Tet-GBP1 plasmids (Fisch *et al*, 2019a) were mutated using site-directed mutagenesis and transduced into the THP-1 Δ*GBP1*+Tet target cells using Lentiviral transduction as described before (Fisch *et al*, 2019a). Similarly, to make cells expressing YFP-*CASP4*^{C258S} and mutated GBP1 versions, THP-1 Δ*GBP1*+Tet-mCH-*GBP1*^{K51A}, +Tet-mCH-*GBP1*^{C589A} or +Tet-mCH-*GBP1*$^{\Delta589\text{-}592}$ (Fisch *et al*, 2019a) were transduced with pMX-CMV-YFP-*CASP4*^{C258S} (Fisch *et al*, 2019a) using lentiviral particles

Creation of YFP-CASP5 expressing cell line

To create catalytically-inactive caspase-5^{C315S}, the ORF of pMX-CASP5 (kind gift of Mitchel Pallett) (Munday *et al*, 1995; Eckhart *et al*, 2006) was mutated by site-directed mutagenesis and confirmed by Sanger sequencing. Next the CASP5^{C315S} ORF was amplified by PCR and used for Gibson assembly into XhoI digested pMX-CMV-YFP (Eldridge *et al*, 2017) to create pMX-CMV-YFP-*CASP5*^{C315S} expression vector.

Caspase-5 encoding plasmids and the packaging plasmids pCMV-MMLV-pack (Shenoy *et al*, 2012) and pVSVg were transfected into HEK293T cells in serum-free DMEM using Lipofectamine 2000 (11668019, Thermo Scientific) at a ratio of 5:4:1. Medium was replaced 12 h post-transfection with fresh DMEM + 10% FBS to rest the cells. Medium was replaced again after 12 h with complete DMEM containing 5 mM sodium butyrate to boost virus production and left for another 12 h. Medium was replaced with RPMI + 10% FBS and the cells left to produce lentiviral particles for one day. Virus containing supernatant was filtered through a 0.43 µm syringe filter and supplemented with 8 µM polybrene. The THP-1 Δ*GBP1*+Tet-mCH-*GBP1* target cells were then resuspended in 500 µL of the virus containing medium and 'spinfected' for 30 mins at 720 x g before being placed back in the incubator. One hour p.i. 1 mL complete medium was added, and the cells left to rest. This infection procedure was repeated for a total of three times before selection with 1 µg/mL Puromycin. Once untransduced control cells had died in the selection medium, the newly created cells were tested by immunoblotting.

Creation of myc-AIM2 expressing cell line

To create a lentiviral vector for constitutive expression of myc-AIM2, the ORF was amplified from pcDNA3-myc-AIM2 (Addgene #73958, a gift from Christian Stehlik) (Khare *et al*, 2014) and Gibson assembled into BstBI and BsrGI digested pLEX-MCS-ASC-GFP (Addgene #73957, a gift from Christian Stehlik) (de Almeida *et al*, 2015) to create pLEX-MCS-myc-AIM2. The newly made vector was then transduced into THP-1 +Tet-*CASP8*-FLAG cells to create THP-1 +Tet-*CASP8* + myc-*AIM2* cells using Lentiviral transduction as described above.

Fixed immunofluorescence microscopy

For confocal imaging 0.25x10^6 THP-1 cells were seeded on gelatin-coated (G1890, Sigma) coverslips in 24-well plates. Following differentiation, treatments and infection, cells were washed three times with warm PBS prior to fixation to remove any uninvaded pathogens and then fixed with 4% methanol-free formaldehyde (28906, Thermo Scientific) for 15 min at room temperature. Following fixation, cells were washed again with PBS and kept at 4°C overnight to quench any unreacted formaldehyde. Fixed specimens were permeabilized with PermQuench buffer (0.2% (w/v) BSA and 0.02% (w/v) saponin in PBS) for 30 minutes at room temperature and then stained with primary antibodies for one hour at room temperature. After three washes with PBS, cells were incubated with the appropriated secondary antibody and 1 µg/mL Hoechst 33342 (H3570, Invitrogen) diluted in PermQuench buffer for 1 hour at room temperature. Cells were washed with PBS five times and mounted using 5 µL Mowiol.

Specimens were imaged on a Leica SP5-inverted confocal microscope using 100x magnification and analyzed using LAS-AF software. For structured-

illumination super-resolution imaging, specimens were imaged on a GE Healthcare Lifesciences DeltaVision OMX SR imaging system and images reconstructed using the DeltaVision software. All images were further formatted using FIJI software. 3D rendering of image stacks and distance measurements of *AIM2-ASC-CASP8* inflammasome specks was performed using Imaris 8.3.1.

Quantification of protein recruitment to pathogen vacuoles and ASC speck formation

Cells seeded as above were infected with *Tg* MOI = 1 or STm MOI = 30 and fixed at indicated times p.i. Nuclei were stained with Hoechst33342 (H3570, Invitrogen), proteins with antibodies and appropriate secondary antibody and coverslips mounted as described above. Images were acquired using a Ti-E Nikon microscope equipped with LED-illumination and an Orca-Flash4 camera using a 60x magnification. All intracellular parasites/bacteria of 100 fields of view were automatically counted based on whether they show recruitment of the protein of interest using HRMAn high-content image analysis (Fisch *et al*, 2019b). Further, the analysis pipeline was used to measure the fluorescence intensity of GBP1 on STm vacuoles using the radial intensity measurement implemented in HRMAn.

For quantification of ASC speck formation, 100 *Tg*-infected cells were manually counted per condition using a Ti-E Nikon microscope equipped with LED-illumination using 60x magnification based on whether they contain an ASC speck and whether STm was decorated with GBP1/CASP4. The experiment was repeated independently three times.

EdU labeling for visualization of *Tg*-DNA release

Type I (RH) *Tg* were grown in fully confluent and non-replicating HFFs for 3 days in the presence of 20 µM EdU to incorporate the nucleotide into their DNA. Labelled parasites were then harvested and used for infection as described above. 6 hours p.i. cells were fixed and EdU incorporated into *Tg*-DNA visualized by staining the specimens using Click-iT™ EdU Cell Proliferation Kit for Imaging, Alexa Fluor™ 647 dye (C10340, Invitrogen) according to the manufacturers instruction. Coverslips were further stained with Hoechst and mounted before imaging on a Ti-E Nikon microscope equipped with LED-illumination and an Orca-Flash4 camera using a 100x magnification.

Correlative light and electron microscopy

$1.25x10^6$ THP-1 cells were seeded in a µ-Dish35 mm, high Glass Bottom Grid-500 (81168, ibidi) and differentiated with PMA as described before. Cells were then pre-stimulated with IFNγ overnight and infected with type II (Pru) *Tg* at an MOI of one for 6 hours. One hour prior to fixation, 1 µg/mL CellMask Deep Red (C10046, Invitrogen) and 20 µM Hoechst 33342 (H3570, Invitrogen) was added to the culture medium to label the cells for detection in fluorescence microscopy. Cells were fixed by adding warm 8% (v/v) formaldehyde (Taab Laboratory Equipment Ltd) in 0.2 M phosphate buffer (PB) pH 7.4 directly to the cell culture medium (1:1) for 15min. The samples were then washed and imaged in PB using a Zeiss AiryScan LSM 880 confocal microscope. Samples were then processed using a Pelco BioWave Pro+ microwave (Ted Pella Inc) and following a protocol adapted from the National Centre for Microscopy and Imaging Research protocol (Deerinck *et al*, 2010) (See **Table 4** for full BioWave program details). Each step was performed in the Biowave, except for the PB and water wash steps, which consisted of two washes followed by two washes in the Biowave without vacuum (at 250 W for 40 s). All chemical incubations were performed in the Biowave for 14 min under vacuum in 2 min cycles alternating with/without 100 W power. The SteadyTemp plate was set to 21ºC unless otherwise stated. In brief, the samples were fixed again in 2.5% (v/v) glutaraldehyde (Taab) / 4% (v/v) formaldehyde in 0.1 M PB. The cells were then stained with 2% (v/v) osmium tetroxide (Taab) / 1.5% (v/v) potassium ferricyanide (Sigma), incubated in 1% (w/v) thiocarbohydrazide (Sigma) with SteadyTemp plate set to 40ºC, and further stained with 2% osmium tetroxide in ddH_2O (w/v). The cells were then incubated in 1% aqueous uranyl acetate (Agar Scientific), and then washed in dH_2O with SteadyTemp set to 40ºC for both steps. Samples were then stained with Walton's lead aspartate with SteadyTemp set to 50ºC and dehydrated in a graded ethanol series (70%, 90%, and 100%, twice each), at 250 W for 40 s without vacuum. Exchange into Durcupan ACM® resin (Sigma) was performed in 50% resin in ethanol, followed by 4 pure Durcupan steps, at 250 W for 3 min, with vacuum cycling (on/off at 30 s intervals), before embedding at 60ºC for 48 h. Blocks were serial sectioned using a UC7 ultramicrotome (Leica Microsystems) and 70 nm sections were picked up on Formvar-coated slot copper grids (Gilder Grids Ltd). Consecutive sections were viewed using a 120 kV Tecnai G2 Spirit transmission electron microscope (Thermo Fischer Scientific) and images were captured using an Orius CCD camera (Gatan Inc). Individual TEM images of ~25-30 consecutive sections per *Tg* parasite were converted as Tiff in Digital Micrograph (Gatan Inc.) and aligned using TrakEM2, a plugin of the FIJI framework (Cardona *et al*, 2012). The stacks were used to check the integrity of the PV and for course alignment with the AiryScan data.

Vacuole breakage assay (HRMAn)

For quantification of *Tg* vacuole integrity, cells seeded in black-wall 96-well imaging plates were infected and treated as described before. One hour prior to fixation, 1 µg/mL CellMask Deep Red (C10046, Invitrogen) was added to the culture medium to load the cytosol of host cells with this fluorescent dye. Following fixation and staining with Hoechst (H3570, Invitrogen), plates were imaged at 40x magnification on a CellInsight CX7 High-

Content Screening (HCS) Platform (Thermo Scientific) and 25 fields of view per well were recorded. Fluorescence of the dye within detected *Tg* vacuoles was then analyzed using HRMAn (Fisch *et al*, 2019b). Additionally, HRMAn was used to classify *Tg* vacuoles based on recruitment of mCH-GBP1 using the implemented neural network and the dataset stratified into decorated and non-decorated vacuoles.

Differential stain for detection of cytosolic STm

To distinguish between STm contained in vacuoles and bacteria that had escaped into the cytosol of infected macrophages, cells were differentially permeabilized using 25 µg/mL digitonin for one minute at room temperature as has been described before (Meunier & Broz, 2015). Cytosolic STm were then stained using anti-Salmonella antibody (ab35156, Abcam) that has been pre-labelled using Alexa Fluor™ 647 Protein Labeling Kit (A20173, Invitrogen) for 15 minutes at 37°C, prior to immediate fixation with 4% paraformaldehyde. Following fixation cells were permeabilized as described above and all STm were stained using the same but unlabeled antibody and corresponding Alexa-488 labelled secondary antibody. Cells were further stained with Hoechst (H3570, Invitrogen) and imaged on a Leica SP5-inverted confocal microscope using 100x magnification. For quantification, 100 fields of view per coverslip (typically >1000 individual STm overall) were acquired using a Ti-E Nikon microscope equipped with LED-illumination and an Orca-Flash4 camera at 60x magnification and analyzed with HRMAn (Fisch *et al*, 2019b) for colocalization of fluorescent signal of all and cytosolic STm.

Data handling and statistics

Data analysis used nested t-test, one-way ANOVA or two-way ANOVA as groups that were compared are indicated in the figure legends. Benjamini, Krieger and Yekutieli false-discovery rate (Q = 5%) based correction for multiple comparisons as implemented in Prism was used when making more than 3 comparisons. Graphs were plotted using Prism 8.1.1 (GraphPad Inc.) and presented as means of n = 3 experiments (with usually 3 technical repeats within each experiment) with error bars representing SEM, unless stated otherwise.

REFERENCES

de Almeida L, Khare S, Misharin A V., Patel R, Ratsimandresey RA, Wallin MC, Perlman H, Greaves DR, Hoffman HM, Dorfleutner A & Stehlik C (2015) The PYRIN domain-only protein POP1 inhibits inflammasome assembly and ameliorates inflammatory disease. *Immunity* **43:** 264

Baker PJ, Boucher D, Bierschenk D, Tebartz C, Whitney PG, D'Silva DB, Tanzer MC, Monteleone M, Robertson AAB, Cooper MA, Alvarez-Diaz S, Herold MJ, Bedoui S, Schroder K & Masters SL (2015) NLRP3 inflammasome activation downstream of cytoplasmic LPS recognition by both caspase-4 and caspase-5. *Eur. J. Immunol.* **45:** 2918–2926

Bierschenk D, Monteleone M, Moghaddas F, Baker PJ, Masters SL, Boucher D & Schroder K (2019) The *Salmonella* pathogenicity island-2 subverts human NLRP3 and NLRC4 inflammasome responses. *J. Leukoc. Biol.* **105:** 401–410

Bradfield C (2016) Sulfated DAMPs mobilize human GBPs for cell-autonomous immunity against bacterial pathogens. *PhD thesis, Yale University, New Haven, CT*

Cardona A, Saalfeld S, Schindelin J, Arganda-Carreras I, Preibisch S, Longair M, Tomancak P, Hartenstein V & Douglas RJ (2012) TrakEM2 Software for Neural Circuit Reconstruction. *PLoS One* **7:** e38011

Coers J (2017) Sweet host revenge: Galectins and GBPs join forces at broken membranes. *Cell. Microbiol.* **19:** e12793

Deerinck TJ, Bushong E, Thor A, Ellisman M, Deerinck T, Thor A, Deerinck T, Bushong E, Thor CA & Ellisman M (2010) NCMIR methods for 3D EM: A new protocol for preparation of biological specimens for serial block face scanning electron microscopy. *Microscopy*

Degrandi D, Kravets E, Konermann C, Beuter-Gunia C, Klumpers V, Lahme S, Wischmann E, Mausberg AK, Beer-Hammer S & Pfeffer K (2013) Murine Guanylate Binding Protein 2 (mGBP2) controls Toxoplasma gondii replication. *Proc. Natl. Acad. Sci.* **110:** 294–299

Eckhart L, Kittel C, Gawlas S, Gruber F, Mildner M, Jilma B & Tschachler E (2006) Identification of a novel exon encoding the amino-terminus of the predominant caspase-5 variants. *Biochem. Biophys. Res. Commun.* **348:** 682–688

Eldridge MJG, Sanchez-Garrido J, Hoben GF, Goddard PJ & Shenoy AR (2017) The Atypical Ubiquitin E2 Conjugase UBE2L3 Is an Indirect Caspase-1 Target and Controls IL-1β Secretion by Inflammasomes. *Cell Rep.* **18:** 1285–1297

Feeley EM, Pilla-Moffett DM, Zwack EE, Piro AS, Finethy R, Kolb JP, Martinez J, Brodsky IE & Coers J (2017) Galectin-3 directs antimicrobial guanylate binding proteins to vacuoles furnished with bacterial secretion systems. *Proc. Natl. Acad. Sci.* **114:** E1698–E1706

Fisch D, Bando H, Clough B, Hornung V, Yamamoto M, Shenoy AR & Frickel E (2019a) Human GBP1 is a microbe-specific gatekeeper of macrophage apoptosis and pyroptosis. *EMBO J.* **38:** e100926

Fisch D, Yakimovich A, Clough B, Wright J, Bunyan M, Howell M, Mercer J & Frickel E (2019b) Defining host–pathogen interactions employing an artificial intelligence workflow. *Elife* **8:** e40560

Gaidt MM, Ebert TS, Chauhan D, Schmidt T, Schmid-Burgk JL, Rapino F, Robertson AAB, Cooper MA, Graf T & Hornung V (2016) Human Monocytes Engage an Alternative Inflammasome Pathway. *Immunity* **44:** 833–846

Gomes MTR, Cerqueira DM, Guimarães ES, Campos PC & Oliveira SC (2019) Guanylate-binding proteins at the crossroad of noncanonical inflammasome activation during bacterial infections. *J.*

Leukoc. Biol. **106:** 553–562

Huang S, Meng Q, Maminska A & MacMicking JD (2019) Cell-autonomous immunity by IFN-induced GBPs in animals and plants. *Curr. Opin. Immunol.* **60:** 71–80

Jorgensen I, Rayamajhi M & Miao EA (2017) Programmed cell death as a defence against infection. *Nat. Rev. Immunol.* **17:** 151–164

Kagan JC, Magupalli VG & Wu H (2014) SMOCs: supramolecular organizing centres that control innate immunity. *Nat. Rev. Immunol.* **14:** 821

Khare S, Ratsimandresey RA, de Almeida L, Cuda CM, Rellick SL, Misharin A V, Wallin MC, Gangopadhyay A, Forte E, Gottwein E, Perlman H, Reed JC, Greaves DR, Dorfleutner A & Stehlik C (2014) The PYRIN domain-only protein POP3 inhibits ALR inflammasomes and regulates responses to infection with DNA viruses. *Nat. Immunol.* **15:** 343–53

Kravets E, Degrandi D, Ma Q, Peulen T-O, Klümpers V, Felekyan S, Kühnemuth R, Weidtkamp-Peters S, Seidel CA & Pfeffer K (2016) Guanylate binding proteins directly attack Toxoplasma gondii via supramolecular complexes. *Elife* **5:** e11479

Lagrange B, Benaoudia S, Wallet P, Magnotti F, Provost A, Michal F, Martin A, Di Lorenzo F, Py BF, Molinaro A & Henry T (2018) Human caspase-4 detects tetra-acylated LPS and cytosolic Francisella and functions differently from murine caspase-11. *Nat. Commun.* **9:** 242

Liu BC, Sarhan J, Panda A, Muendlein HI, Ilyukha V, Coers J, Yamamoto M, Isberg RR & Poltorak A (2018) Constitutive Interferon Maintains GBP Expression Required for Release of Bacterial Components Upstream of Pyroptosis and Anti-DNA Responses. *Cell Rep.* **24:** 155-168.e5

MacMicking JD (2012) Interferon-inducible effector mechanisms in cell-autonomous immunity. *Nat. Rev. Immunol.* **12:** 367–382

Man SM, Hopkins LJ, Nugent E, Cox S, Glück IM, Tourlomousis P, Wright JA, Cicuta P, Monie TP & Bryant CE (2014) Inflammasome activation causes dual recruitment of NLRC4 and NLRP3 to the same macromolecular complex. *Proc. Natl. Acad. Sci. U. S. A.* **111:** 7403–8

Man SM, Karki R, Malireddi RKS, Neale G, Vogel P, Yamamoto M, Lamkanfi M & Kanneganti T (2015) The transcription factor IRF1 and guanylate-binding proteins target activation of the AIM2 inflammasome by Francisella infection. *Nat. Immunol.* **16:** 467–475

Man SM, Place DE, Kuriakose T & Kanneganti T-D (2017) Interferon-inducible guanylate-binding proteins at the interface of cell-autonomous immunity and inflammasome activation. *J. Leukoc. Biol.* **101:** 143–150

Man SM, Tourlomousis P, Hopkins L, Monie TP, Fitzgerald KA & Bryant CE (2013) Salmonella infection induces recruitment of Caspase-8 to the inflammasome to modulate IL-1β production. *J. Immunol.* **191:** 5239–46

Meunier E & Broz P (2015) Quantification of Cytosolic vs. Vacuolar Salmonella in Primary Macrophages by Differential Permeabilization. *J. Vis. Exp.*: e52960

Meunier E, Wallet P, Dreier RF, Costanzo S, Anton L, Rühl S, Dussurgey S, Dick MS, Kistner A, Rigard M, Degrandi D, Pfeffer K, Yamamoto M, Henry T & Broz P (2015) Guanylate-binding proteins promote activation of the AIM2 inflammasome during infection with Francisella novicida. *Nat. Immunol.* **16:** 476–84

Miao EA, Leaf IA, Treuting PM, Mao DP, Dors M, Sarkar A, Warren SE, Wewers MD & Aderem A (2010) Caspase-1-induced pyroptosis is an innate immune effector mechanism against intracellular bacteria. *Nat. Immunol.* **11:** 1136–42

Mordue DG & Sibley LD (1997) Intracellular fate of vacuoles containing Toxoplasma gondii is determined at the time of formation and depends on the mechanism of entry. *J. Immunol.* **159:** 4452–4459

Mostowy S & Shenoy AR (2015) The cytoskeleton in cell-autonomous immunity: structural determinants of host defence. *Nat. Rev. Immunol.* **15:** 559–73

Munday NA, Vaillancourt JP, Ali A, Casano FJ, Miller DK, Molineaux SM, Yamin TT, Yu VL & Nicholson DW (1995) Molecular cloning and pro-apoptotic activity of ICErelII and ICErelIII, members of the ICE/CED-3 family of cysteine proteases. *J. Biol. Chem.* **270:** 15870–6

Naschberger E, Geißdörfer W, Bogdan C, Tripal P, Kremmer E, Stürzl M & Britzen-Laurent N (2017) Processing and secretion of guanylate binding protein-1 depend on inflammatory caspase activity. *J. Cell. Mol. Med.* **20:** 1–13

Praefcke G (2018) Regulation of innate immune functions by guanylate-binding proteins. *Int. J. Med. Microbiol.* **308:** 237–245

Prakash B, Renault L, Praefcke GJ, Herrmann C & Wittinghofer A (2000) Triphosphate structure of guanylate-binding protein 1 and implications for nucleotide binding and GTPase mechanism. *EMBO J.* **19:** 4555–64

Qin A, Lai D-H, Liu Q, Huang W, Wu Y-P, Chen X, Yan S, Xia H, Hide G, Lun Z-R, Ayala FJ & Xiang AP (2017) Guanylate-binding protein 1 (GBP1) contributes to the immunity of human mesenchymal stromal cells against Toxoplasma gondii. *Proc. Natl. Acad. Sci.* **114:** 1365–1370

Randow F, MacMicking JD & James LC (2013) Cellular self-defense: how cell-autonomous immunity protects against pathogens. *Science (80-.).* **340:** 701–706

Sanchez-Garrido J, Sancho-Shimizu V & Shenoy AR (2018) Regulated proteolysis of p62/SQSTM1 enables differential control of autophagy and nutrient sensing. *Sci. Signal.* **11:** eaat6903

Sanjana NE, Shalem O & Zhang F (2014) Improved vectors and genome-wide libraries for CRISPR screening. *Nat. Methods* **11:** 783–784

Santos JC & Broz P (2018) Sensing of invading pathogens by GBPs: At the crossroads between cell-autonomous and innate immunity. *J. Leukoc. Biol.* **104:** 729–735

Selleck EM, Fentress SJ, Beatty WL, Degrandi D, Pfeffer K, Virgin HW, MacMicking JD & Sibley LD (2013) Guanylate-binding Protein 1 (Gbp1) Contributes to Cell-autonomous Immunity against Toxoplasma gondii. *PLoS Pathog.* **9:** e1003320

Shenoy AR, Wellington DA, Kumar P, Kassa H, Booth CJ, Cresswell P & MacMicking JD (2012) GBP5 Promotes NLRP3 Inflammasome Assembly and Immunity in Mammals. *Science (80-.).* **336:** 481–485

Shi J, Zhao Y, Wang Y, Gao W, Ding J, Li P, Hu L & Shao F (2014) Inflammatory caspases are innate immune receptors for intracellular LPS. *Nature* **514:** 187–192

Shydlovskyi S, Zienert AY, Ince S, Dovengerds C, Hohendahl A, Dargazanli JM, Blum A, Günther SD, Kladt N, Stürzl M, Schauss AC, Kutsch M, Roux A, Praefcke GJK & Herrmann C (2017) Nucleotide-dependent farnesyl switch orchestrates polymerization and membrane binding of human guanylate-binding protein 1. *Proc. Natl. Acad. Sci. U. S. A.* **114:** E5559–E5568

Spanò S & Galán JE (2018) Taking control: Hijacking of Rab GTPases by intracellular bacterial pathogens. *Small GTPases* **9:** 182–191

Stennicke HR & Salvesen GS (1997) Biochemical characteristics of

caspases-3, -6, -7, and -8. *J. Biol. Chem.* **272:** 25719–23

Sugaya K, Seto S, Tsujimura K & Koide Y (2011) Mobility of late endosomal and lysosomal markers on phagosomes analyzed by fluorescence recovery after photobleaching. *Biochem. Biophys. Res. Commun.* **410:** 371–5

Thurston TLM, Matthews SA, Jennings E, Alix E, Shao F, Shenoy AR, Birrell MA & Holden DW (2016) Growth inhibition of cytosolic Salmonella by caspase-1 and caspase-11 precedes host cell death. *Nat. Commun.* **7:** 13292

Thurston TLM, Wandel MP, von Muhlinen N, Foeglein A & Randow F (2012) Galectin 8 targets damaged vesicles for autophagy to defend cells against bacterial invasion. *Nature* **482:** 414–8

Tummers B & Green DR (2017) Caspase-8: regulating life and death. *Immunol. Rev.* **277:** 76–89

Wu Y-H, Kuo W-C, Wu Y-J, Yang K-T, Chen S-T, Jiang S-T, Gordy C, He Y-W & Lai M-Z (2014) Participation of c-FLIP in NLRP3 and AIM2 inflammasome activation. *Cell Death Differ.* **21:** 451–61

Yamamoto M, Okuyama M, Ma JS, Kimura T, Kamiyama N, Saiga H, Ohshima J, Sasai M, Kayama H, Okamoto T, Huang DCS, Soldati-Favre D, Horie K, Takeda J & Takeda K (2012) A cluster of interferon-gamma-inducible p65 gtpases plays a critical role in host defense against toxoplasma gondii. *Immunity* **37:** 302–313

Supplementary Information

This is supplementary information to the preprint manuscript from Fisch *et al*. 2019. Supplementary section contains supplementary tables, supplementary figures and figure legends. All further information is available upon request.

Supplementary tables

Table 1 – Cell lines

Cell line	Source
THP-1 WT	ATCC, TIB-202
HFF	The Francis Crick Institute, Cell Services
HEK293T	The Francis Crick Institute, Cell Services
THP-1 Δ*GBP1*	Fisch *et al*, EMBOJ 2019
THP-1 Δ*GBP1*+Tet-EV	Fisch *et al*, EMBOJ 2019
THP-1 Δ*GBP1*+Tet-*GBP1*	Fisch *et al*, EMBOJ 2019
THP-1 Δ*GBP1*+Tet-mCH-*GBP1*	Fisch *et al*, EMBOJ 2019
THP-1 Δ*GBP1*+Tet-mCH-*GBP1* + YFP-*CASP4*^{C258S}	Fisch *et al*, EMBOJ 2019
THP-1 Δ*GBP1*+Tet-mCH-*GBP1*^{K51A} +YFP-*CASP4*^{C258S}	Newly made cell line
THP-1 Δ*GBP1*+Tet-mCH-*GBP1*^{C589A} +YFP-*CASP4*^{C258S}	Newly made cell line
THP-1 Δ*GBP1*+Tet-mCH-*GBP1*$^{Δ589-592}$ +YFP-*CASP4*^{C258S}	Newly made cell line
THP-1 WT+Tet-*CASP8*-FLAG	Newly made cell line
THP-1 WT+Tet-*CASP8*-FLAG + myc-*AIM2*	Newly made cell line
THP-1 Δ*GBP1*+Tet-mCH-*GBP1* + YFP-*CASP5*^{C315S}	Newly made cell line
THP-1 Δ*GBP1*+Tet-mCH-*GBP1*^{D192E}	Newly made cell line
THP-1 Δ*GBP1*+Tet-*GBP1*^{D192E}	Newly made cell line

Table 2 – Antibodies

Abbreviations: CST = Cell Signalling Technologies, IB = immunoblot, IF = immunofluorescence

Antibody	Source	Use
Rab7	CST, #9367	IF
Galectin-8	R&D Systems, AF1305	IF
STm-LPS	Abcam, ab8274	IF
FLAG M2	Millipore, F3165	IF, IB
ASC	Adipogen, AG-25B-0006	IF
c-myc	Millipore, M2435	IF, IB
STm	Abcam, ab35156	IF
GBP1	Home-made	IB
CASP1	Adipogen, AG-20B-0048	IB
β -Actin	Sigma, A5316	IB
CASP8	CST, #9746	IB
mCherry	Abcam, ab167453	IB
YFP	Abcam, ab6556	IB
CASP5	CST, #46680	IB
AIM2	CST, #12948	IB

Table 3 – Primers

Name	Sequence 5'-3'	Purpose
BB_CASP 8-fwd	TGCGGCCGCACCATGGGCGGTAGGCGTGTAC	Amplify *CASP8* ORF for cloning into pTet backbone
Flag_CAS P8-rev	GTGGTCCTTATAGTCATCAGAAGGGAAGACAAGTTTTTTTCTTAGTGTGAA AG	
Casp-8_Flag-fwd	GTCTTCCCTTCTGATGACTATAAGGACCACGACGG	Amplify FLAG-tag for cloning into pTet backbone with *CASP8* ORF
pTet-Flag-rev	GATCGATCAGGGATCCTACTTATCGTCATCGTCTTTGTAATCAATATC	
GBP1-D192E-fwd	CCCTGGACTTGGAAGCAGAGGGACAACCCC	Mutate *GBP1* ORF
GBP1-D192E-rev	GGGACCTGAACCTTCGTCTCCCTGTTGGGG	
CASP5_ C315S-fwd	CATCATTGTCCAGGCCTCCAGAGGTGAAAAACATG	Mutate *CASP5* ORF
CASP5_ C315S-rev	CATGTTTTTCACCTCTGGAGGCCTGGACAATGATG	
BB_CASP 5-fwd	GTCCGGACTCAGATCTCGAGCTCAAGCTTCGATGTTCAAAGGTATCCTTCA GAGTGGATTGG	Amplify *CASP5* ORF for cloning into pMX-CMV-YFP backbone
BB_CASP 5-rev	CGCGCCGGCCCTCGATCAATTGCCAGGAAAGAGGTAGAAATCTCTTG	
BB-AIM2-fwd	CTCGAGCTCAAGCTTGCCACCATGGAACAGAAACTCATCTCTGAAGAGGAT CTG	Amplify myc-*AIM2* ORF for cloning into pLEX backbone
BB-AIM2-rev	CCGCTTTACTTGTACCCTAGAATAGGGCCCTCTAGATGCATGCTC	

Table 4 – Electron microscopy sample preparation protocol

Description	Step#	Time (min)	Time (sec)	Power (Watts)	SteadyTemp temperature (ºC)	Vacuum cycle vent time (sec)	Vacuum cycle vacuum time (sec)	Vacuum set point (inch Hg)	User Prompt (1 = YES, 0 = NO)	Vacuum OFF (1 = no vacuum, 0 = vacuum)	Vacuum cycle (1 = ON, 0 = OFF)	Vacuum ON (1 = vacuum, 0 = no vacuum)
BENCH STEP Rinse in 0.1M PB	1	0	0	0	21	0	0	0	1	1	0	0
BENCH STEP Rinse in 0.1M PB	2	0	0	0	21	0	0	0	1	1	0	0
Rinse in 0.1M PB	3	0	40	250	21	0	0	0	1	1	0	0
Rinse in 0.1M PB	4	0	40	250	21	0	0	0	1	1	0	0
Osmium ON	5	2	0	100	21	0	0	20	1	0	0	1
Osmium OFF	6	2	0	0	21	0	0	20	0	0	0	1
Osmium ON	7	2	0	100	21	0	0	20	0	0	0	1
Osmium OFF	8	2	0	0	21	0	0	20	0	0	0	1
Osmium ON	9	2	0	100	21	0	0	20	0	0	0	1
Osmium OFF	10	2	0	0	21	0	0	20	0	0	0	1
Osmium ON	11	2	0	100	21	0	0	20	0	0	0	1
BENCH STEP Rinse in water	12	0	0	0	21	0	0	0	1	1	0	0
BENCH STEP Rinse in water	13	0	0	0	21	0	0	0	1	1	0	0
Rinse in water	14	0	40	250	21	0	0	0	1	1	0	0
Rinse in water	15	0	40	250	21	0	0	0	1	1	0	0
Thiocarbohydrazide ON	16	2	0	100	40	0	0	20	1	0	0	1
Thiocarbohydrazide OFF	17	2	0	0	40	0	0	20	0	0	0	1
Thiocarbohydrazide ON	18	2	0	100	40	0	0	20	0	0	0	1
Thiocarbohydrazide OFF	19	2	0	0	40	0	0	20	0	0	0	1
Thiocarbohydrazide ON	20	2	0	100	40	0	0	20	0	0	0	1
Thiocarbohydrazide OFF	21	2	0	0	40	0	0	20	0	0	0	1
Thiocarbohydrazide ON	22	2	0	100	40	0	0	20	0	0	0	1
BENCH STEP Rinse in water	23	0	0	0	21	0	0	0	1	1	0	0
BENCH STEP Rinse in water	24	0	0	0	21	0	0	0	1	1	0	0
Rinse in water	25	0	40	250	21	0	0	0	1	1	0	0
Rinse in water	26	0	40	250	21	0	0	0	1	1	0	0
Osmium ON	27	2	0	100	21	0	0	20	1	0	0	1
Osmium OFF	28	2	0	0	21	0	0	20	0	0	0	1
Osmium ON	29	2	0	100	21	0	0	20	0	0	0	1
Osmium OFF	30	2	0	0	21	0	0	20	0	0	0	1
Osmium ON	31	2	0	100	21	0	0	20	0	0	0	1
Osmium OFF	32	2	0	0	21	0	0	20	0	0	0	1
Osmium ON	33	2	0	100	21	0	0	20	0	0	0	1
BENCH STEP Rinse in water	34	0	0	0	21	0	0	0	1	1	0	0
BENCH STEP Rinse in water	35	0	0	0	21	0	0	0	1	1	0	0
Rinse in water	36	0	40	250	21	0	0	0	1	1	0	0
Rinse in water	37	0	40	250	21	0	0	0	1	1	0	0
Uranyl acetate ON	38	2	0	100	40	0	0	20	1	0	0	1
Uranyl acetate OFF	39	2	0	0	40	0	0	20	0	0	0	1
Uranyl acetate ON	40	2	0	100	40	0	0	20	0	0	0	1
Uranyl acetate OFF	41	2	0	0	40	0	0	20	0	0	0	1
Uranlyl acetate ON	42	2	0	100	40	0	0	20	0	0	0	1
Uranyl acetate OFF	43	2	0	0	40	0	0	20	0	0	0	1
Uranyl acetate ON	44	2	0	100	40	0	0	20	0	0	0	1
BENCH STEP Rinse in water	45	0	0	0	40	0	0	0	1	1	0	0
BENCH STEP Rinse in water	46	0	0	0	40	0	0	0	1	1	0	0
Rinse in water	47	0	45	250	40	0	0	0	1	1	0	0
Rinse in water	48	0	45	250	40	0	0	0	1	1	0	0
Lead aspartate ON	49	2	0	100	50	0	0	20	1	0	0	1
Lead aspartate OFF	50	2	0	0	50	0	0	20	0	0	0	1
Lead aspartate ON	51	2	0	100	50	0	0	20	0	0	0	1
Lead aspartate OFF	52	2	0	0	50	0	0	20	0	0	0	1
Lead aspartate ON	53	2	0	100	50	0	0	20	0	0	0	1
Lead aspartate OFF	54	2	0	0	50	0	0	20	0	0	0	1
Lead aspartate ON	55	2	0	100	50	0	0	20	0	0	0	1
BENCH STEP Rinse in water	56	0	0	0	21	0	0	0	1	1	0	0
BENCH STEP Rinse in water	57	0	0	0	21	0	0	0	1	1	0	0
Rinse in water	58	0	45	250	21	0	0	0	1	1	0	0
Rinse in water	59	0	45	250	21	0	0	0	1	1	0	0
70% Ethanol ON	60	0	40	250	21	0	0	0	1	1	0	0
70% Ethanol ON	61	0	40	250	21	0	0	0	1	1	0	0
90% Ethanol ON	62	0	40	250	21	0	0	0	1	1	0	0
90% Ethanol ON	63	0	40	250	21	0	0	0	1	1	0	0
100% Ethanol ON	64	0	40	250	21	0	0	0	1	1	0	0
100% Ethanol ON	65	0	40	250	21	0	0	0	1	1	0	0
50% Resin ON	66	3	0	250	21	30	30	20	1	0	1	0
100% Resin ON	67	3	0	250	21	30	30	20	1	0	1	0
100% Resin ON	68	3	0	250	21	30	30	20	1	0	1	0
100% Resin ON	69	3	0	250	21	30	30	20	1	0	1	0
100% Resin ON	70	3	0	250	21	30	30	20	1	0	1	0
TURN SYSTEM OFF	71	0	0	0	21	0	0	0	0	1	0	0

Supplementary Figures

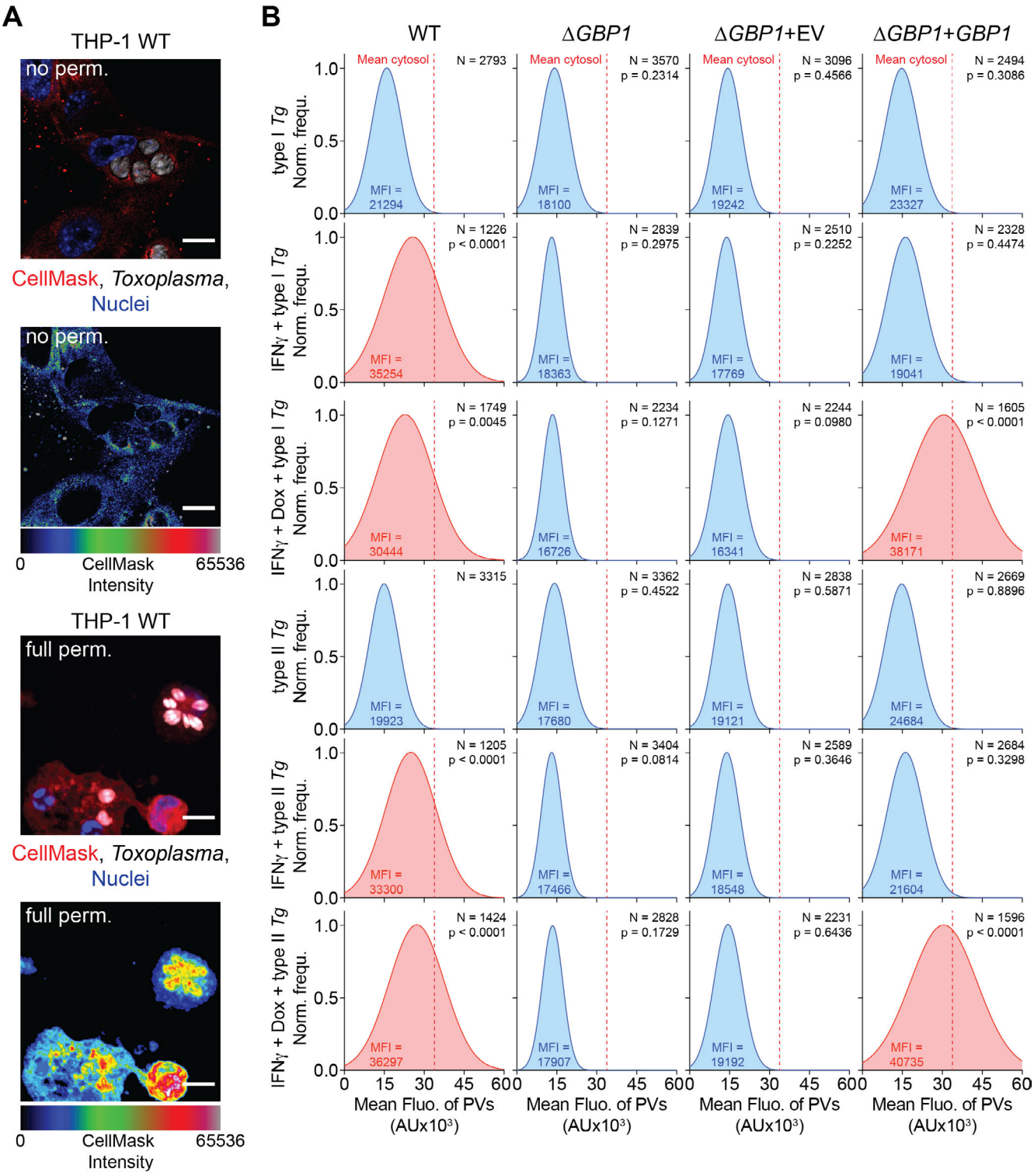

Figure S1 (related to Figure 1): Macrophages open Toxoplasma vacuoles which leads to flooding with a cytosolic fluorescent dye.
(A) Representative immunofluorescence images from THP-1 WT infected with type I *Toxoplasma gondii* (*Tg*) for 18 hours and stained with CellMask but not permeabilized (no perm.; **Top**) fully permeabilized with saponin (full perm.; **Bottom**). Rainbow intensity diagram of the CellMask signal from images used for quantification. Red: CellMask; Grey: *Tg*; Blue: Nuclei. Scale bars 10 µm. **(B)** Representative normalised frequency plots (Norm. frequ.) of fluorescence intensities of vacuoles in type I or type II *Tg*-infected THP-1 WT, THP-1 Δ*GBP1*, THP-1 Δ*GBP1*+Tet-empty vector (EV) or THP-1 Δ*GBP1*+Tet-*GBP1* cells treated with IFNγ, Doxycycline (Dox) or left untreated and stained with CellMask. Mean fluorescence signal of the cytosol indicated by dashed red line and mean fluorescence intensity of the vacuoles (MFI) displayed in the graphs in Fig 1A. Conditions with increased mean intensity of the vacuole fluorescence are highlighted in red. N = number of vacuoles. **Data information:** *P* values in **(B)** from nested one-way ANOVA comparing means of n = 3 independent experiments from indicated condition to untreated WT cells.

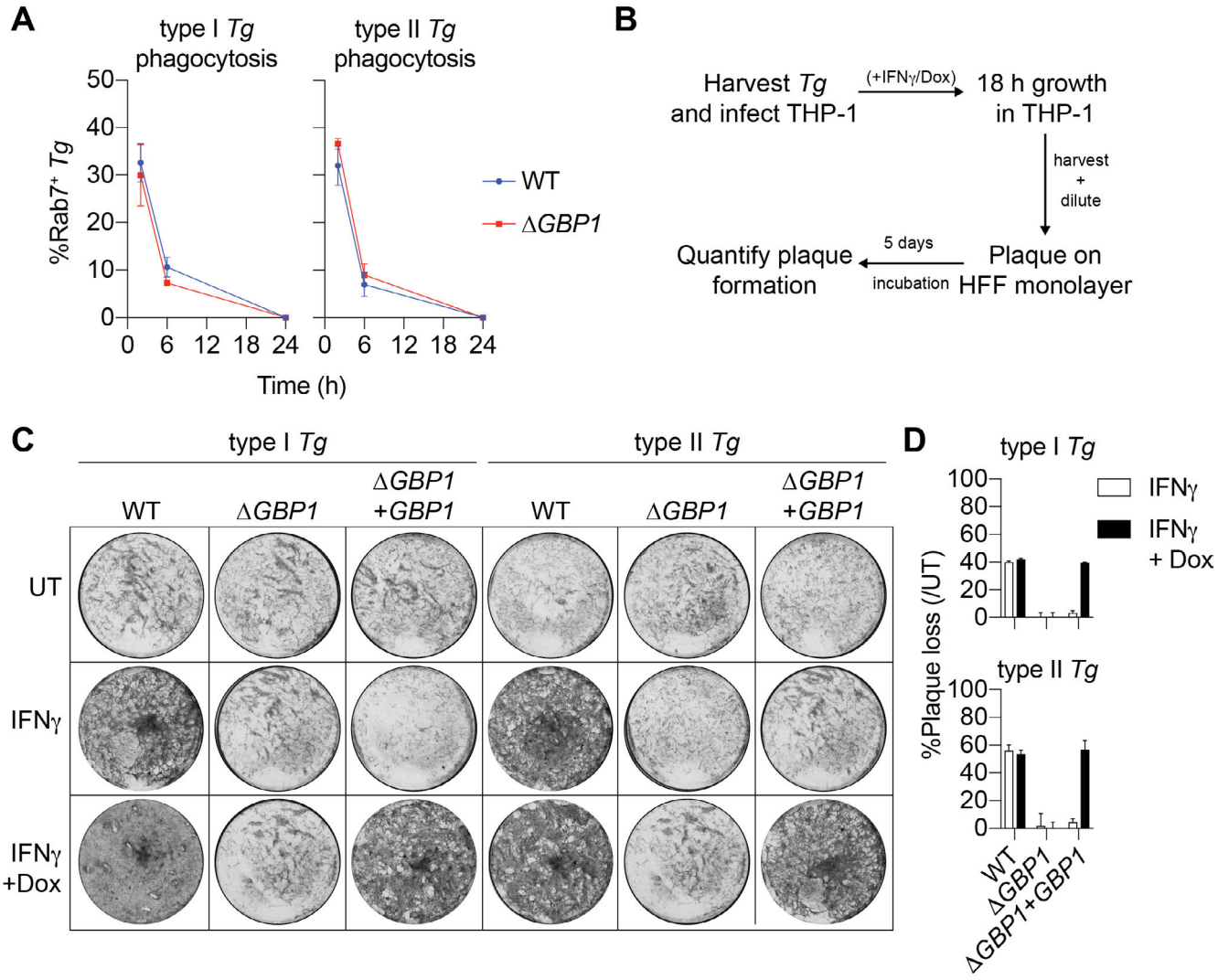

Figure S2 (related to Figure 1): *Toxoplasma* is phagocytosed by macrophages and GBP1 controls pathogen growth.
(A) Quantification of Toxoplasma gondii (*Tg*) phagocytosis by THP-1 WT and THP-1 Δ*GBP1* cells pre-treated with IFNγ and infected with type I or type II *Tg* for the indicated amounts of time. Phagosomes were scored based on the recruitment of Rab7 (Rab7^{+}). **(B)** Schematic overview of the workflow for *Tg* plaque assays for parasite viability determination. In brief: *Tg* was harvested and used to infect THP-1 macrophages treated with IFNγ and Doxycycline (Dox). 18 hours post infection the macrophages were lysed, parasites collected from the cells and the supernatant, diluted and used to infect human foreskin fibroblast (HFF) monolayers and left for 4-5 days until plaques were detected. **(C)** Representative images of *Tg* plaques on HFFs in wells of a 24-well plate after 18 hours of culture in THP-1 cells of the indicated genotype and treatment. UT; untreated. **(D)** Quantification of plaque loss following *Tg* culture in THP-1 cells for 18 hours. Data presents the reduction in plaque area of the indicated treatment normalised to the untreated (UT) condition. **Data information:** Graphs in **(A+D)** show mean ± SEM from n = 3 independent experiments.

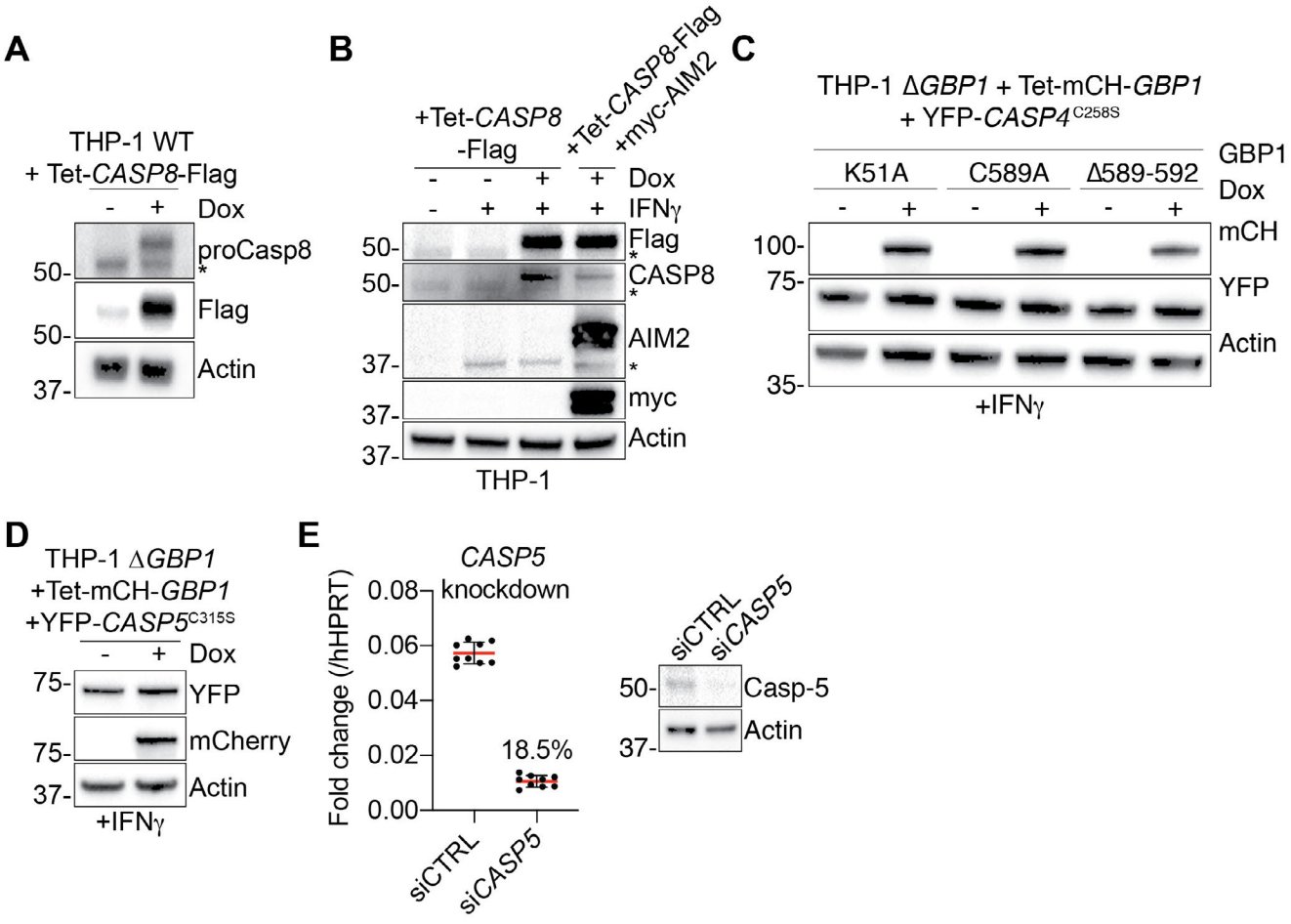

Figure S3 (Related to Figures 3+4): Quality control of cell lines and knockdowns
(A) Representative immunoblots for proCaspase-8, FLAG and β-actin from THP-1 +Tet-*CASP8*-FLAG cells showing Dox-inducible caspase-8-Flag expression. Cells were treated with Doxycycline (Dox) as indicated or left untreated. * endogenous caspase-8. **(B)** Representative immunoblots for FLAG, caspase-8 (CASP8), AIM2, myc and β-actin from THP-1 WT, THP-1 +Tet-*CASP8*-FLAG and THP-1 +Tet-*CASP8*-FLAG+myc-*AIM2* cells showing Dox-inducible caspase-8-Flag expression and constitutive expression of myc-AIM2. Cells were treated with IFNγ, Dox or left untreated as indicated. * endogenous proteins. **(C)** Representative immunoblots for mCherry, YFP and β-actin from THP-1 Δ*GBP1*+Tet-mCH-*GBP1* cells expressing the indicated mutant of GBP1 and also stably expressing YFP-*CASP4*^{C258S}. Cells were primed with IFNγ and treated with Dox as indicated. **(D)** Representative immunoblots for mCherry (mCH), YFP and β-actin from THP-1 Δ*GBP1*+Tet-mCH-*GBP1* +YFP-*CASP5*^{C315S}. Cells were primed with IFNγ and treated with Dox as indicated. **(E)** **Left:** RT-qPCR and **Right:** representative immunoblot of THP-1 WT cells transfected with non-targeting control (CTRL) siRNA or siRNA against caspase-5 (*CASP5*). Indicated percentage shows remaining transcript level in si*CASP5* transfected cells as compared to CTRL. **Data information:** Graph in **(E)** shows mean ± SEM from n = 9 independent experiments.

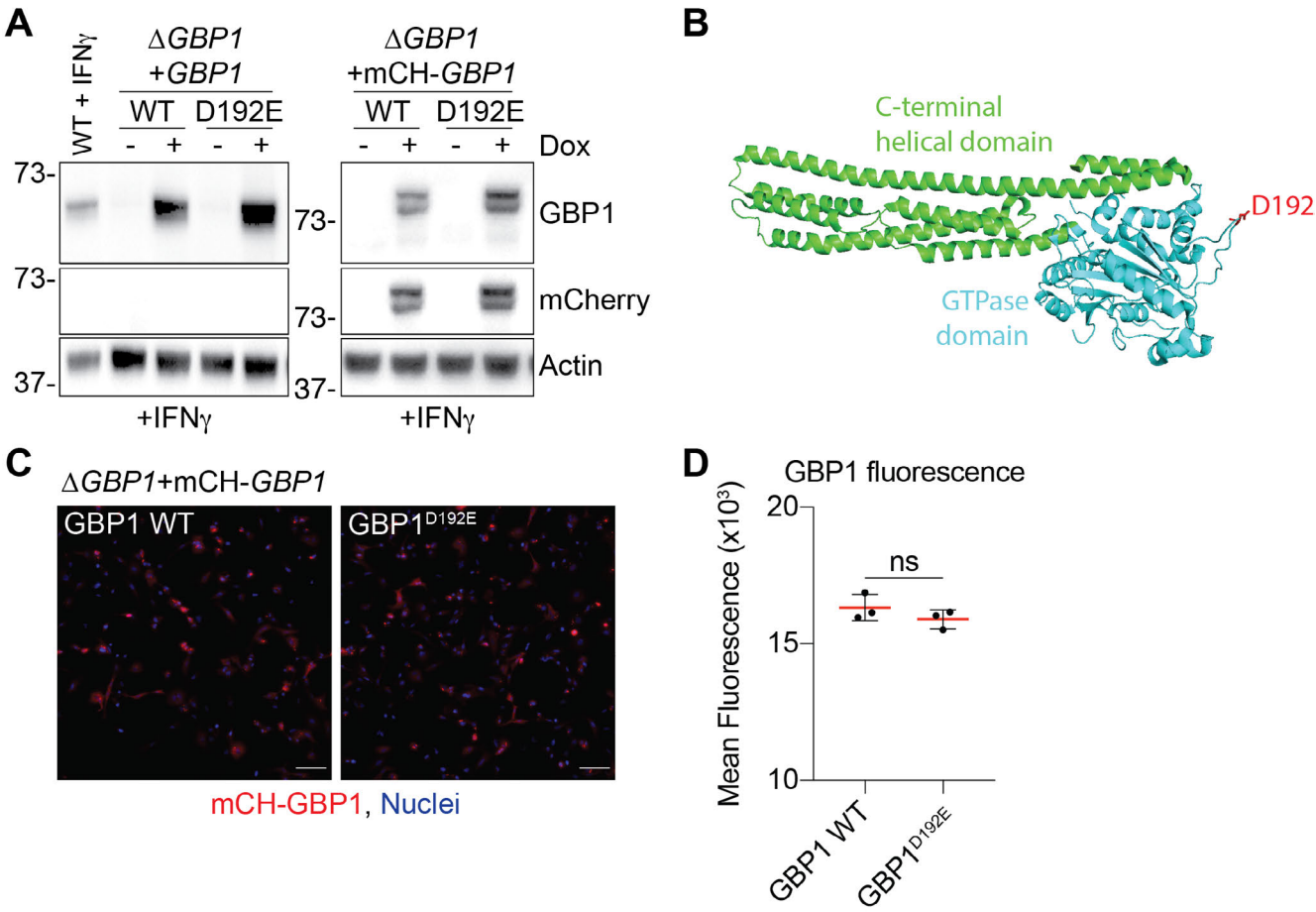

Figure S4 (Related to Figure 5): Characterisation of THP-1 cell lines expressing GBP1^{D192E}
(A) Representative immunoblots of GBP1, mCherry (mCH) and β-actin from IFNγ-primed THP-1 Δ*GBP1*+Tet-*GBP1* or *GBP1*^{D192E} with and without mCh-tag for Doxycycline (Dox)-inducible expression. Cells were treated with Dox as indicated. **(B)** Crystal structure of human GBP1 (PDB: 1F5N) with GTPase domain highlighted in cyan, C-terminal helical domain in green and aspartate D192 in red. **(C)** Representative images from THP-1 Δ*GBP1*+Tet-mCH-*GBP1* **(Left)** or +Tet-*GBP1*^{D192E} **(Right)** cells treated with IFNγ and Dox to induce GBP1 expression. Red: mCh-GBP1; Blue: Nuclei. Scale bars 100 µm. **(D)** Quantification of mean mCH-GBP1 or mCH-GBP1^{D192E} fluorescence per cell from 100 fields of view. Data shows individual values from n = 3 independent experiments and mean (red line) ± SEM. **Data information:** *P* values in **(D)** from t-test comparing means of n = 3 independent experiments. ns, not significant.